

Group 4 permethylindenyl complexes for slurry-phase polymerisation of ethylene

Jessica V. Lamb, Jean-Charles Buffet, Zoë R. Turner and Dermot O'Hare*

Received 00th January 20xx,
Accepted 00th January 20xx

DOI: 10.1039/x0xx00000x

www.rsc.org/

A series of ten well-defined group 4 *ansa*-bridged permethylindenyl (C_9Me_7 , Ind*, I*) complexes have been prepared, fully characterised and supported on inorganic solid supports. These catalysts were investigated in the slurry-phase polymerisation of ethylene. A range of inorganic solid supports have been utilised; solid polymethylaluminoxane (sMAO), MAO modified layered double hydroxide (LDHMAO) and MAO modified silica (SSMAO). The sMAO supported catalytic systems exhibit some of the highest slurry-phase polymerisation activities reported in literature with activities reaching $9509 \text{ kg}_{PE} \text{ mol}_M^{-1} \text{ h}^{-1} \text{ bar}^{-1}$ for $Me_2SB(Cp^{Me}, I^*)ZrMe_2$ at 80°C after 5 minutes of polymerisation; 34% more active than an industrial standard under similar conditions. These systems produce polyethylenes with low molecular weights, M_w , reaching as low as 46 kg mol^{-1} for $E\text{-}Me_2SB(Cp^{nBu}, I^*)ZrCl_2$ at 90°C after 30 minutes of polymerisation with a uniform, mono-disperse "popcorn" morphology. The sMAO supported systems show much higher catalytic activities and much more industrially desirable polyethylene morphology than the same complexes supported on LDHMAO and SSMAO.

Introduction

Surface-supported metallocene catalysts offer a key alternative to traditional Ziegler-Natta and Phillips ethylene polymerisation catalysts.^{1, 2} Their single-site nature allows for fine-tuning of polymer properties,³ such as molecular weights, co-monomer incorporation, molecular weights distribution and polymer stereochemistry.⁴ Industrially, metallocene catalysts are commonly employed in heterogeneous systems,⁵ utilising inorganic supports such as clays,⁶ silicas,^{7,8} magnesium chloride,^{2,9} alumina,⁵ and zeolites.¹⁰

Group 4 metallocenes (Cp_2MX_2) are d^0 organometallic compounds containing two η^5 -cyclopentadienyl-type ligands and two σ -type ligands. The ancillary Cp ligands can be varied to form asymmetric metallocene compounds with remarkable efficiency as α -olefin polymerisation catalysts.^{11–13} *Ansa*-bridges can be employed between the two Cp substituents to prevent ligand rotation and enforce complex rigidity;¹⁴ with a higher catalytic activity accompanying increased reaction space at the metal centre and reduced steric hinderance of the ligand.^{15, 16} The adaptability of Cp_2MX_2 -type complexes results in highly tuneable, stereo-rigid metallocenes with a wide range of catalytic reactivity.^{8, 17, 18} Slight variations of the ring substituents and bridging groups can greatly influence catalytic activity, with electronic structure and spatial organisation of the

active site having profound effects on the resulting polymer properties.^{16, 19, 20}

The indenyl ligand (C_9H_7 , Ind, I) is a common alternative to Cp. Its capacity to undergo an η^5 - η^3 ring slip allows the metal to lose electrons in its valence shell without changing oxidation state; resulting in increased substitution rates at the metal centre. Supported early group 4 $Cp^R_2MX_2$ ($M = Ti$) catalysts displayed low ethylene polymerisation activities.^{1, 21} However, replacement of the Cp substituent with Ind increased the activity, stereospecificity and thermal stability of the supported catalyst.^{22, 23} Permethylation of the indenyl ring (C_9Me_7 , Ind*, I*) can lead to enhanced complex stability, attributed to inductive donation and increased steric bulk around the metal centre.²⁴ A Ind*H derivative, hexamethyl indenyl (C_9Me_6H , Ind#, I#),²⁵ is of particular interest as a synthetic precursor to *ansa*-bridged ligand frameworks. We recently reported a range of unsymmetrical *ansa*-bridged I* compounds (Chart 1).^{26, 27}

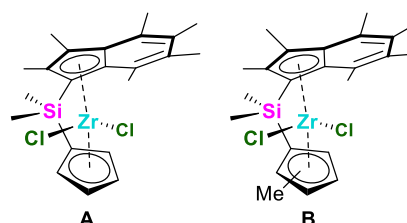


Chart 1. Previous reported related group 4 permethylindenyl complexes ($Me_2SB(Cp, I^*)ZrCl_2$ (A) and $Me_2SB(Cp^{Me}, I^*)ZrCl_2$ (B)).^{26, 27}

Synthesis and characterisation of $Me_2SB(Cp^{nBu}, I^*)Li_2$

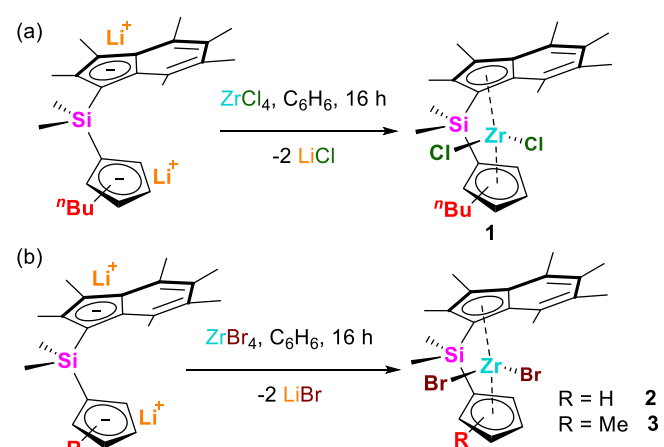
Chemistry Research Laboratory, Department of Chemistry, University of Oxford, 12 Mansfield Road, OX1 3TA, Oxford, UK. E-mail: dermot.ohare@chem.ox.ac.uk; Tel: +44 (0)1865 272686.

*Electronic Supplementary Information (ESI) available: General details, NMR spectroscopy, crystallographic data and definitions of structural parameters, and additional polymerisation data. See DOI: 10.1039/x0xx00000x

$\text{Me}_2\text{SB}(\text{Cp}^{n\text{Bu}}, \text{I}^*)\text{Li}_2$ was prepared following a previously reported one pot procedure for the preparation of $\text{Me}_2\text{SB}(\text{Cp}^{\text{R}}, \text{I}^*)\text{Li}_2$ ($\text{R} = \text{H}, \text{Me}$).^{26,27} The reaction of $\text{Ind}^*\text{SiMe}_2\text{Cl}$ with $\text{LiCp}^{n\text{Bu}}$ followed by deprotonation with 2.2 equivalents $n\text{BuLi}$ afforded $\text{Me}_2\text{SB}(\text{Cp}^{n\text{Bu}}, \text{I}^*)\text{Li}_2$ as a pale orange powder in 30% yield after work-up. The ^1H NMR spectrum shows a 50:50 mixture of starting materials and products; it is noted that increased stirring time and heating was unsuccessful in driving the reaction to completion. Multiplets corresponding to the Cp protons are observed at 6.43–6.91 ppm, with the six singlets at 2.30–3.08 ppm corresponding to the indenyl ring methyl groups, the singlet at approximately 1.0 ppm attributed to the silicon methyl groups and the multiplets at 0.88, 1.48, 1.79 and 2.83 ppm corresponding to the protons on the *n*-butyl chain.

Synthesis and characterisation of $\text{Me}_2\text{SB}(\text{Cp}^{\text{R}}, \text{I}^*)\text{ZrX}_2$

Equimolar quantities of $\text{Me}_2\text{SB}(\text{Cp}^{n\text{Bu}}, \text{I}^*)\text{Li}_2$ and freshly dried ZrCl_4 were stirred in benzene at room temperature for 16 hours. Following work-up, $\text{Z-Me}_2\text{SB}(\text{Cp}^{n\text{Bu}}, \text{I}^*)\text{ZrCl}_2$ (**Z-1**) and $\text{E-Me}_2\text{SB}(\text{Cp}^{n\text{Bu}}, \text{I}^*)\text{ZrCl}_2$ (**E-1**) were isolated as orange solids in 0.5 and 0.9% yield respectively (Scheme 1a). Dilithium salts $\text{Me}_2\text{SB}(\text{Cp}^{\text{R}}, \text{I}^*)\text{Li}_2$ ($\text{R} = \text{H}, \text{Me}$) were prepared according to a literature procedure^{26,27} and reacted with one equivalent ZrBr_4 to form $\text{Me}_2\text{SB}(\text{Cp}, \text{I}^*)\text{ZrBr}_2$ (**2**) and $\text{Me}_2\text{SB}(\text{Cp}^{\text{Me}}, \text{I}^*)\text{ZrBr}_2$ (**3**) in 57 and 48% yield respectively (Scheme 1b). Akin to analogous $\text{Me}_2\text{SB}(\text{Cp}^{\text{Me}}, \text{I}^*)\text{ZrCl}_2$ (**B**),^{26,27} **3** forms as a 60:40 isomeric mixture of two isomers with the methyl group occupying the least sterically hindered *gamma* positions of the cyclopentadienyl ring. The ^1H NMR spectra of **1-3** (Fig. S1, S3, S5, S7) show multiplets of equal intensity between 5.08 and 6.80 ppm corresponding to the Cp protons, singlets between 1.86 and 2.61 ppm corresponding to the methyl groups on the indenyl ring and resonances between 0.53 and 0.64 ppm corresponding to the silyl methyl groups. The ^1H NMR spectra of **E-1** and **Z-1** show multiplets corresponding to protons on the *n*-butyl chain (Fig. S1 and S3), while the ^1H NMR spectra of **3** shows an additional methyl peak for each isomer corresponding to the methyl group on the Cp ring (Fig. S7).

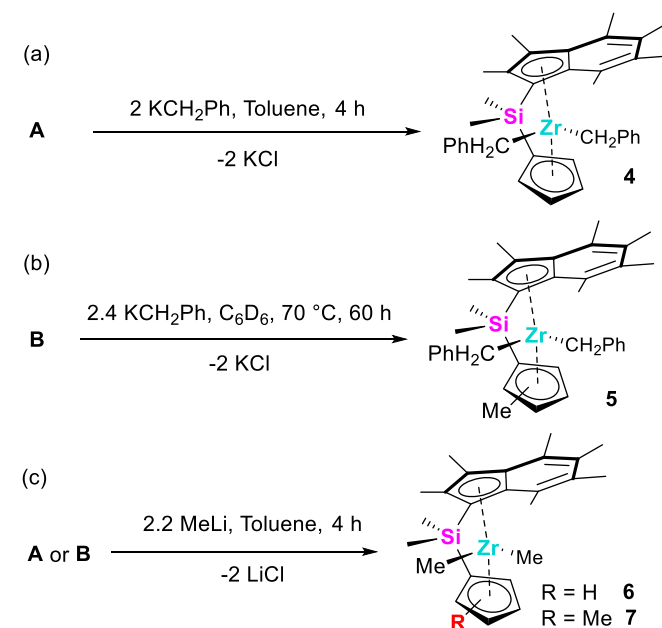


Scheme 1. Synthesis of (a) $\text{Me}_2\text{SB}(\text{Cp}^{n\text{Bu}}, \text{I}^*)\text{ZrCl}_2$ (**1**) and (b) $\text{Me}_2\text{SB}(\text{Cp}^{\text{R}}, \text{I}^*)\text{ZrBr}_2$ ($\text{R} = \text{H}$ (**2**), Me (**3**)).

The solid-state structures of **E-1**, **Z-1** and **2** were obtained from saturated pentane solutions at -34°C . Their molecular structures are depicted in Fig. 1, with selected bond lengths and angles presented in Tables 1 and S1. The steric parameters show good agreement with each other, and with previously reported unsymmetrical I^* *ansa*-bridged zirconocenes.^{26,27} Of note, is the slightly longer $\text{Zr-Cp}^{\text{R}}_{\text{cent}}$ distance of $\text{Z-Me}_2\text{SB}(\text{Cp}^{n\text{Bu}}, \text{I}^*)\text{ZrCl}_2$ (**Z-1**) when compared to $\text{Z-Me}_2\text{SB}(\text{Cp}^{\text{Me}}, \text{I}^*)\text{ZrCl}_2$ (**Z-B**) (2.2143(1) and 2.1935(1) Å respectively), caused by the increased steric bulk of the *n*-butyl chain positioned under the I^* ring in **Z-1** compared to the methyl group of **Z-B**. **Z-1** also experiences a larger ring tilt angle (α) than **Z-B**, indicative of a less sterically hindered metal centre implying that **Z-1** experiences less strain due to the *ansa*-bridge. **Z-1** has steric parameters in very good agreement with related zirconocene $\text{Me}_2\text{SB}(\text{Cp}, \text{I})\text{ZrCl}_2$, with similar $\text{Zr-Ind}_{\text{cent}}$ of 2.227(5) Å, $\text{Zr-Cp}_{\text{cent}}$ of 2.198(5) Å and δ of $126.9(1)^\circ$ for $\text{Me}_2\text{SB}(\text{Cp}, \text{I})\text{ZrCl}_2$.²⁸ **Z-1** and **E-1** show very good agreement with each other and have very similar steric parameters. Of interest is the relative position of the *n*-butyl chain in both isomers; the plane *n*-butyl chain of **E-1** lies near-perpendicular to the plane of the Cp ring (87.89°), however in **Z-1** the *n*-butyl chain is almost in the plane of the Cp ring (14.51°) (Fig. S27). $\text{Me}_2\text{SB}(\text{Cp}, \text{I}^*)\text{ZrBr}_2$ (**2**) displays steric parameters in good agreement with analogous $\text{Me}_2\text{SB}(\text{Cp}, \text{I}^*)\text{ZrCl}_2$ (**A**), however displays a longer Zr-X distance (average distance of 2.626 and 2.441 Å respectively) due to the weaker electrostatic attraction between Zr and Br.

Synthesis and characterisation of $\text{Me}_2\text{SB}(\text{Cp}^{\text{R}}, \text{I}^*)\text{ZrR}'_2$ ($\text{R} = \text{H}, \text{Me}$; $\text{R}' = \text{Me}, \text{CH}_2\text{Ph}$)

There are several motives for the movement away from halide leaving groups and towards alkyls.



Scheme 2. Synthesis of (a) $\text{Me}_2\text{SB}(\text{Cp}, \text{I}^*)\text{Zr}(\text{CH}_2\text{Ph})_2$ (**4**), (b) $\text{Me}_2\text{SB}(\text{Cp}^{\text{Me}}, \text{I}^*)\text{Zr}(\text{CH}_2\text{Ph})_2$ (**5**) and (c) $\text{Me}_2\text{SB}(\text{Cp}, \text{I}^*)\text{ZrMe}_2$ ($\text{R} = \text{H}$ (**6**), Me (**7**)) where **A** is $\text{Me}_2\text{SB}(\text{Cp}, \text{I}^*)\text{ZrCl}_2$ and **B** is $\text{Me}_2\text{SB}(\text{Cp}^{\text{Me}}, \text{I}^*)\text{ZrCl}_2$.

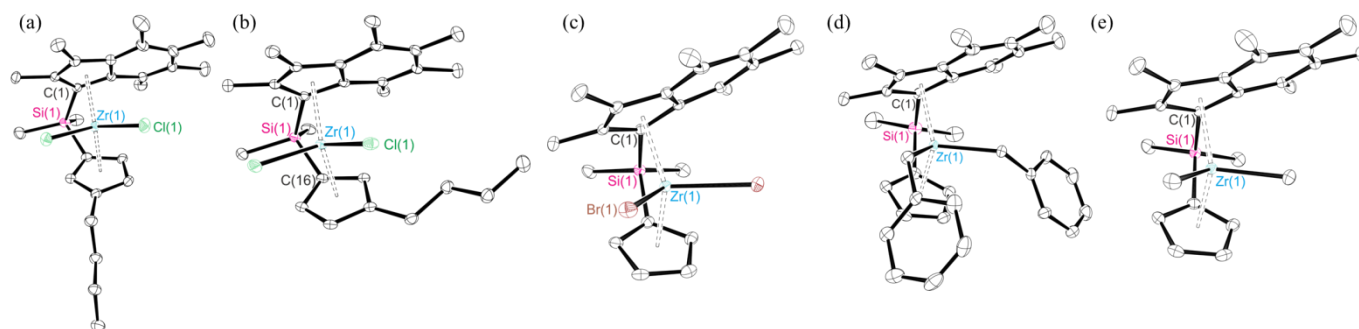


Fig. 1 Solid-state molecular structures of (a) E - $\text{Me}_2\text{SB}(\text{Cp}^{\text{nBu}}, \text{I}^*)\text{ZrCl}_2$ (**E-1**), (b) Z - $\text{Me}_2\text{SB}(\text{Cp}^{\text{nBu}}, \text{I}^*)\text{ZrCl}_2$ (**Z-1**), (c) $\text{Me}_2\text{SB}(\text{Cp}, \text{I}^*)\text{ZrBr}_2$ (**2**), (d) $\text{Me}_2\text{SB}(\text{Cp}, \text{I}^*)\text{Zr}(\text{CH}_2\text{Ph})_2$ (**4**) and (e) $\text{Me}_2\text{SB}(\text{Cp}, \text{I}^*)\text{ZrMe}_2$ (**6**). Ellipsoids are given at 50% probability.

Table 1. Selected bond lengths (Å) and angles (°) for complexes **A**, **B**, **E-1**, **Z-1**, **2**, **4** and **6**. *defined in Table S1.

	Complex	Zr(1)- Cp ^R _{cent} (Å)	Zr(1)- I [*] _{cent} (Å)	$\alpha(^{\circ})^*$	$\Delta(^{\circ})^*$	Reference
A	$\text{Me}_2\text{SB}(\text{Cp}, \text{I}^*)\text{ZrCl}_2$	2.2076(1)	2.2244(1)	60.19	126.37(1)	26
E-B	E - $\text{Me}_2\text{SB}(\text{Cp}^{\text{Me}}, \text{I}^*)\text{ZrCl}_2$	2.2194(1)	2.2202(1)	62.38	126.12(1)	26
Z-B	Z - $\text{Me}_2\text{SB}(\text{Cp}^{\text{Me}}, \text{I}^*)\text{ZrCl}_2$	2.1935(1)	2.2202(1)	56.85	130.60(1)	26
E-1	E - $\text{Me}_2\text{SB}(\text{Cp}^{\text{nBu}}, \text{I}^*)\text{ZrCl}_2$	2.2011(1)	2.2308(1)	60.20	127.49(1)	This work
Z-1	Z - $\text{Me}_2\text{SB}(\text{Cp}^{\text{nBu}}, \text{I}^*)\text{ZrCl}_2$	2.2143(1)	2.2200(1)	60.25	126.98(1)	This work
2	$\text{Me}_2\text{SB}(\text{Cp}, \text{I}^*)\text{ZrBr}_2$	2.2012(1)	2.2300(1)	60.14	126.32(1)	This work
4	$\text{Me}_2\text{SB}(\text{Cp}, \text{I}^*)\text{Zr}(\text{CH}_2\text{Ph})_2$	2.1943(1)	2.2615(1)	59.80	126.88(1)	This work
6	$\text{Me}_2\text{SB}(\text{Cp}, \text{I}^*)\text{ZrMe}_2$	2.2201(1)	2.2442(1)	59.16	126.96(1)	This work

Mechanistically, employing a methyl leaving group ($\text{Me}_2\text{SB}(\text{Cp}^{\text{R}}, \text{I}^*)\text{ZrMe}_2$) enables reaction with other co-catalysts, such the strong Lewis acid $\text{B}(\text{C}_6\text{F}_5)_3$, to form the active cationic species $[\text{Me}_2\text{SB}(\text{Cp}^{\text{R}}, \text{I}^*)\text{ZrMe}]^+$.²⁹ The bisbenzyl complexes $\text{Me}_2\text{SB}(\text{Cp}^{\text{R}}, \text{I}^*)\text{Zr}(\text{CH}_2\text{Ph})_2$ ($\text{R} = \text{H}$ (**4**), Me (**5**)) were initially targeted due to the enhanced slurry-phase ethylene polymerisation activity of *meso*-(EBI^{*}) $\text{Zr}(\text{CH}_2\text{Ph})_2$ compared to *meso*-(EBI^{*}) ZrCl_2 .³⁰

$\text{Me}_2\text{SB}(\text{Cp}, \text{I}^*)\text{ZrCl}_2$ (**A**) and $\text{Me}_2\text{SB}(\text{Cp}^{\text{Me}}, \text{I}^*)\text{ZrCl}_2$ (**B**) were synthesised according to a literature procedure; as reported **B** was obtained as a 60:40 mixtures of two isomers with the methyl group at the *gamma* positions of the Cp ring.²⁶ Reaction of stoichiometric quantities of **A** and KCH_2Ph at room temperature afforded $\text{Me}_2\text{SB}(\text{Cp}, \text{I}^*)\text{Zr}(\text{CH}_2\text{Ph})_2$ (**4**) as a yellow solid in 38% yield (Scheme 2a), while the reaction of $\text{Me}_2\text{SB}(\text{Cp}^{\text{Me}}, \text{I}^*)\text{ZrCl}_2$ (**B**) with 2.4 equivalents of KCH_2Ph at 70 °C yielded $\text{Me}_2\text{SB}(\text{Cp}^{\text{Me}}, \text{I}^*)\text{Zr}(\text{CH}_2\text{Ph})_2$ (**5**) as an orange oil in 78% yield (Scheme 2b). Their ^1H NMR spectra (Fig. S9 and S11) show resonances for the silicon methyl, indenyl methyl and cyclopentadienyl protons at 0.53–0.63, 1.57–2.57 and 5.04–6.28 ppm respectively, in addition to resonances at –0.04–2.20 and 6.53–7.25 ppm corresponding to the CH_2 protons on the benzyl chain and the phenyl protons on the benzyl ring respectively. The ^1H NMR spectrum of **5** shows an

additional resonance in the 1.57–2.57 range corresponding to the methyl group on the Cp ring (Fig. S11). It also confirms that the 60:40 isomeric mixture present in the parent dichloro complex is retained in the product.

The salt metathesis reaction of **A** and **B** with 2.2 equivalents of MeLi in toluene lead to the formation of $\text{Me}_2\text{SB}(\text{Cp}, \text{I}^*)\text{ZrMe}_2$ (**6**) and $\text{Me}_2\text{SB}(\text{Cp}^{\text{Me}}, \text{I}^*)\text{ZrMe}_2$ (**7**) in 18 and 72% yield respectively (Scheme 2c). When compared to the parent complexes, the ^1H NMR spectra of **6** and **7** show two additional singlet resonances between –1.28 and –0.13 ppm corresponding to the methyl groups directly bound to the zirconium (Fig. S13, S15). Similarly to the benzyl substituted complex **5**, the ^1H NMR spectrum of **7** shows the 60:40 isomeric mixture of the parent complex is retained.

Yellow crystals of **4** and **6** suitable for a single crystal X-ray diffraction study were obtained from a saturated pentane solution at –34 °C (Fig. 1, Tables 1 and S1). The Zr–Cp_{cent} distance of $\text{Me}_2\text{SB}(\text{Cp}, \text{I}^*)\text{Zr}(\text{CH}_2\text{Ph})_2$ (**4**) is comparable to the parent compound $\text{Me}_2\text{SB}(\text{Cp}, \text{I}^*)\text{ZrCl}_2$ (**A**) (2.1943(1) and 2.2076(1) Å respectively); however, **4** possesses a longer Zr–I^{*}_{cent} distance (2.2615(1) and 2.2244(1) Å respectively) due to the additional steric bulk supplied by the benzyl group. The Zr–Cp_{cent} and Zr–I^{*}_{cent} distances in $\text{Me}_2\text{SB}(\text{Cp}, \text{I}^*)\text{ZrMe}_2$ (**6**) are slightly longer than the parent compound $\text{Me}_2\text{SB}(\text{Cp}, \text{I}^*)\text{ZrCl}_2$ (**A**) (2.2201(1) and

2.2076(1) Å for Zr-Cp_{cent} and 2.2615(1) and 2.2244(1) Å for Zr-I*_{cent} respectively). Both **4** and **6** display smaller Zr-Cp_{cent} distances than an analogous alkyl symmetrical zirconocene *meso*-(EBI*)Zr(CH₂Ph)₂ (average Zr-I*_{cent} of 2.299 Å), most likely due to the decreased steric bulk in the Cp basal ligand when compared to Ind*. **4** and **6** also experience smaller α angles than **A** and *meso*-(EBI*)Zr(CH₂Ph)₂ (59.80, 59.16, 60.19 and 61.85° respectively),³⁰ indicating a more strained system.

Synthesis and characterisation of solid-supported complexes

Three inorganic solid supports were utilised in this work; solid polymethylaluminoxane (sMAO), methylaluminoxane modified layered double hydroxide/Mg₃Al-CO₃ (LDHMAO) and methylaluminoxane modified silica (SSMAO). LDHMAO and SSMAO were prepared according to literature procedures.⁸

Polymeric solid MAO, an insoluble form of oligomeric MAO, has recently been exploited as a solid support for metallocene pre-catalysts in slurry-phase olefin polymerisation,^{18, 30} with activities reaching 6533 kg_{PE} mol_M⁻¹ h⁻¹ bar⁻¹ for *rac*-(EBI)ZrCl₂.³¹ Its structure is relatively undefined; however, recent NMR spectroscopy studies imply a structure featuring long-chain aluminoxane oligomers, with incorporation of “free” TMA and benzoate groups.³¹ MAO-activated aqueous miscible organic solvent treated layered double hydroxides, of formula [M²⁺_{1-x}M³⁺_x(OH)₂]^{x+}(Aⁿ⁻)_{x/n}·bH₂O·c(AMO-solvent), have recently been shown to produce well-defined supports for the immobilisation of single-site olefin polymerisation catalysts.^{32, 33} To this effect, LDHMAO supported *rac*-(EBI)ZrCl₂ has demonstrated slurry-phase ethylene polymerisation activities 25% higher than systems using conventionally synthesised and commercially available LDH supports.³² Silica (SiO₂) is the most

common solid support for the immobilisation of single-site α-olefin polymerisation catalysts.⁵ However, in order to activate the support, silica requires pre-treatment with an alkylaluminium compound, such as methylaluminoxane (MAO), prior to anchoring of the metallocene component. This MAO-modified silica has been well characterised and documented as a solid support for the immobilisation of single-site olefin polymerisation pre-catalysts.^{5, 8, 18, 34-36}

Complex immobilisation was achieved according to a literature procedure.⁸ The complexes **A**, **B**, **4** and **6** were immobilised onto the three inorganic solid supports discussed (sMAO, LDHMAO and SSMAO), with an [Al]₀: [Zr]₀ ratio of 200:1. Complexes **E-1**, **Z-1**, **2**, **3**, **5**, and **7** were immobilised onto sMAO only. The resultant pre-catalysts were obtained as pale purple-pink powders in quantitative yield.

Characterisation of three sMAO supported complexes (**A**_{sMAO}, **4**_{sMAO} and **6**_{sMAO}) was achieved through solid-state NMR spectroscopy (Fig. S17-S25). The ¹³C CP MAS spectra show a major, broad resonance at -8 ppm corresponding to the sMAO methyl environments. By comparison with the solution phase ¹³C{¹H} NMR spectra, the methyl groups on the indene ring can be identified at 15-35 ppm, while the aromatic carbons of the I* ring, cyclopentadienyl carbons and aromatic carbons of the benzyl group are observed at 120-140 ppm. The ²⁹Si CP MAS spectra of **A**_{sMAO}, **4**_{sMAO} and **6**_{sMAO} show a single resonance at approximately -12 ppm corresponding to the bridged silicon atom. The ²⁷Al DPMAS spectra show five resonances at approximately 345, 205, 80, -80, and -240 ppm, corresponding to the different aluminium environments present within solid polymethylaluminoxane.

Table 2. Summary of the slurry-phase polymerisation of ethylene using selected solid polymethylaluminoxane (sMAO) supported pre-catalysts.

Catalyst	[Al] ₀ : [Zr] ₀	Temperature (°C)	Activity (kg _{PE} mol _{Zr} ⁻¹ h ⁻¹ bar ⁻¹)	M _w (kg mol ⁻¹)	M _w /M _n	Ref.
sMAO- <i>rac</i> -(EBI*)ZrCl ₂	200	60	5006	-	-	30
sMAO- <i>meso</i> -(EBI*)ZrCl ₂	300	60	1331	-	-	30
sMAO- <i>meso</i> -(EBI*)Zr(CH ₂ Ph) ₂	300	60	5179	177	2.2	30
sMAO- <i>rac</i> -(SBI*)ZrCl ₂	300	60	5971	183	3.4	-
sMAO-Me ₂ SB(^t Bu ² Flu, I*)ZrCl ₂	200	60	6755	648	2.9	41a
sMAO-Me ₂ SB(^t BuN, I*)TiCl ₂	200	60	3602	490	3.9	41b
A _{sMAO} sMAO-Me ₂ SB(Cp, I*)ZrCl ₂	200	60	7075	140	3.2	This work
4 _{sMAO} sMAO-Me ₂ SB(Cp, I*)Zr(CH ₂ Ph) ₂	200	60	6264	130	3.0	This work
7 _{sMAO} sMAO-Me ₂ SB(Cp ^{Me} , I*)ZrMe ₂	200	60	7948	86	4.0	This work
sMAO-(Cp ⁿ Bu) ₂ ZrCl ₂	200	60	4641	201	2.8	This work

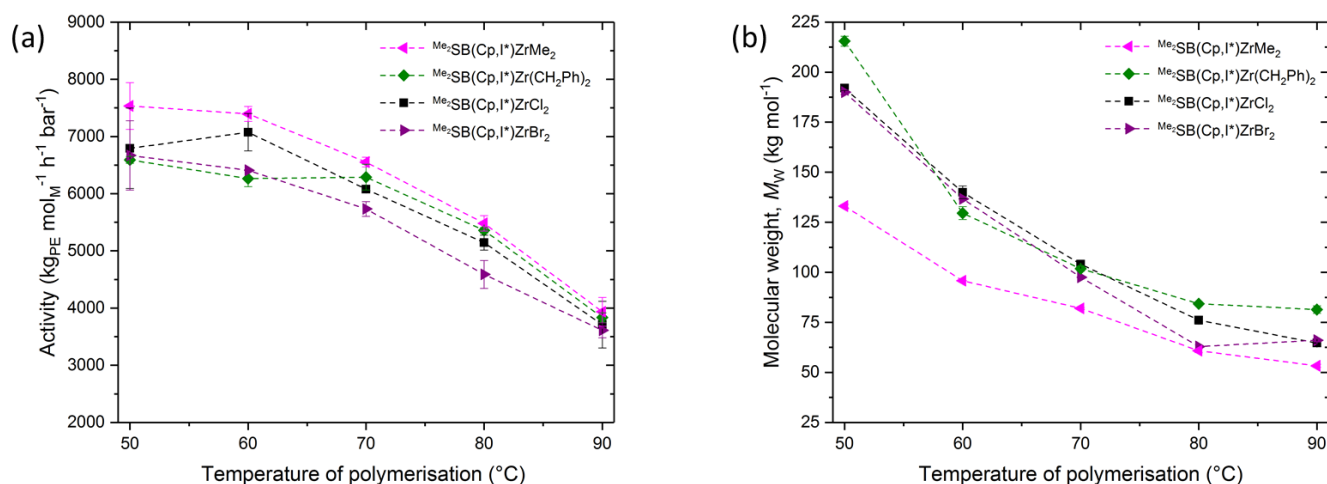


Fig. 2. Slurry-phase ethylene polymerisation (a) activity and (b) molecular weights (M_w) as a function of the temperature of polymerisation. Catalysts in order of decreasing activity at 80 $^{\circ}\text{C}$: $\text{sMAO-Me}_2\text{SB}(\text{Cp}, \text{I}^*)\text{ZrMe}_2$ (**6_{sMAO}**) (pink left triangle), $\text{sMAO-Me}_2\text{SB}(\text{Cp}, \text{I}^*)\text{Zr}(\text{CH}_2\text{Ph})_2$ (**4_{sMAO}**) (green diamond), $\text{sMAO-Me}_2\text{SB}(\text{Cp}, \text{I}^*)\text{ZrCl}_2$ (**A_{sMAO}**) (black square) and $\text{sMAO-Me}_2\text{SB}(\text{Cp}, \text{I}^*)\text{ZrBr}_2$ (**2_{sMAO}**) (purple right triangle). Polymerisation conditions: $[\text{Al}]_0:[\text{Zr}]_0 = 200:1$, 150 mg TiBA scavenger, 2 bar ethylene, 10 mg pre-catalyst, 50 mL hexanes and 30 minutes.

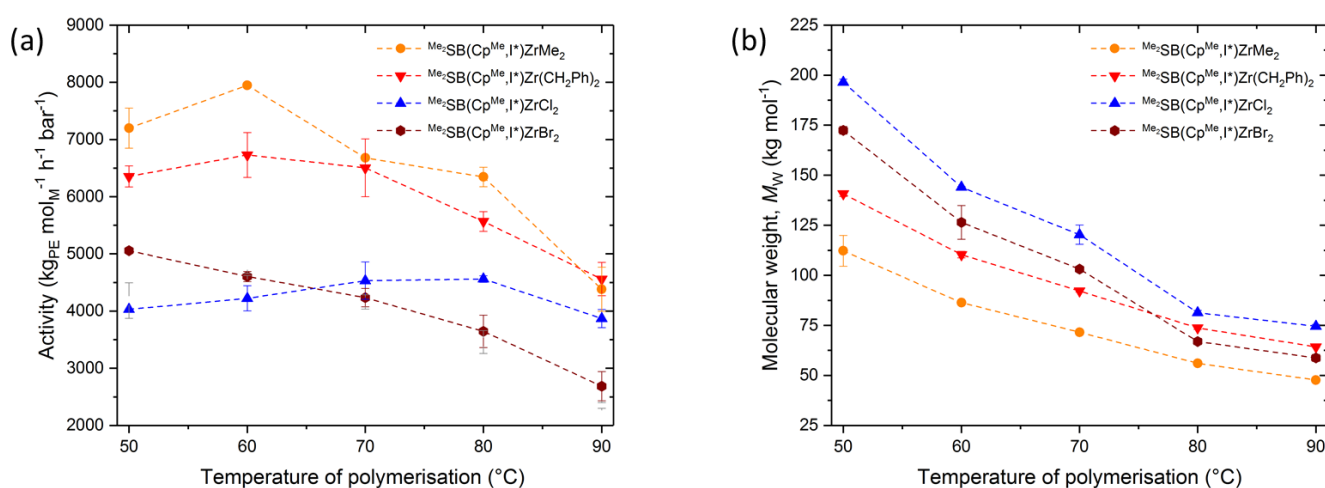


Fig. 3. Slurry-phase ethylene polymerisation (a) activity and (b) molecular weights (M_w) as a function of the temperature of polymerisation. Catalysts in order of decreasing activity at 80 $^{\circ}\text{C}$: $\text{sMAO-Me}_2\text{SB}(\text{Cp}^{\text{Me}}, \text{I}^*)\text{ZrMe}_2$ (**7_{sMAO}**) (orange circle), $\text{sMAO-Me}_2\text{SB}(\text{Cp}^{\text{Me}}, \text{I}^*)\text{Zr}(\text{CH}_2\text{Ph})_2$ (**5_{sMAO}**) (red down triangle), $\text{sMAO-Me}_2\text{SB}(\text{Cp}^{\text{Me}}, \text{I}^*)\text{ZrCl}_2$ (**B_{sMAO}**) (blue up triangle), $\text{sMAO-Me}_2\text{SB}(\text{Cp}^{\text{Me}}, \text{I}^*)\text{ZrBr}_2$ (**3_{sMAO}**) (brown hexagon). Polymerisation conditions: $[\text{Al}]_0:[\text{Zr}]_0 = 200:1$, 150 mg TiBA scavenger, 2 bar ethylene, 10 mg pre-catalyst, 50 mL hexanes and 30 minutes.

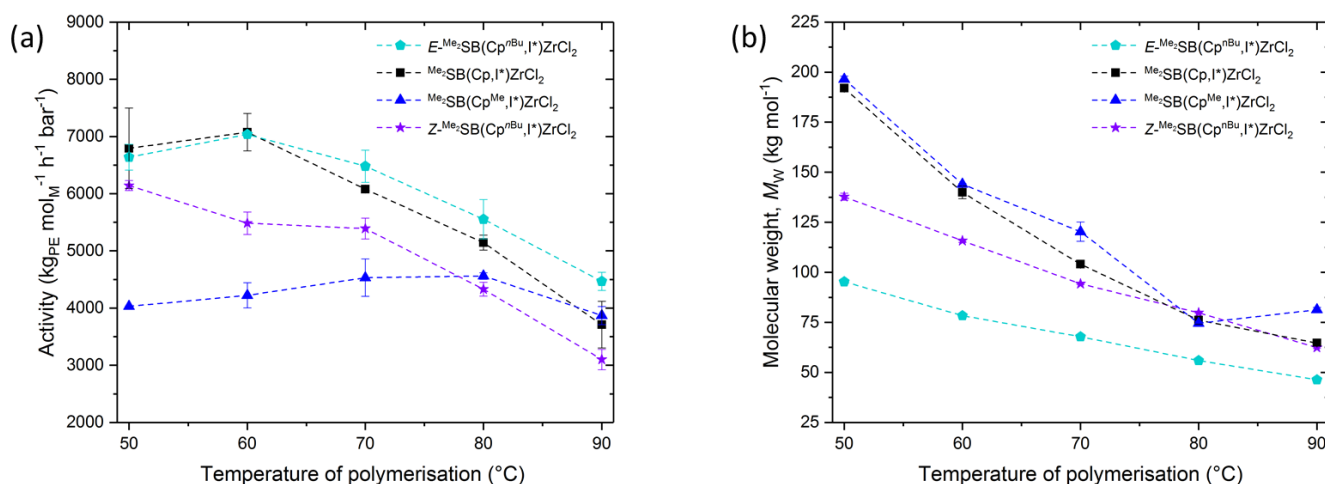


Fig. 4. Slurry-phase ethylene polymerisation (a) activity and (b) molecular weights (M_w) as a function of the temperature of polymerisation. Catalysts in order of decreasing activity at 80 $^{\circ}\text{C}$: $\text{sMAO-E-Me}_2\text{SB}(\text{Cp}^{\text{nBu}}, \text{I}^*)\text{ZrCl}_2$ (**E-1_{sMAO}**) (teal pentagon), $\text{sMAO-Me}_2\text{SB}(\text{Cp}, \text{I}^*)\text{ZrCl}_2$ (**A_{sMAO}**) (black square), $\text{sMAO-Me}_2\text{SB}(\text{Cp}^{\text{Me}}, \text{I}^*)\text{ZrCl}_2$ (**B_{sMAO}**) (blue up triangle), $\text{sMAO-Z-Me}_2\text{SB}(\text{Cp}^{\text{nBu}}, \text{I}^*)\text{ZrCl}_2$ (**Z-1_{sMAO}**) (violet star). Polymerisation conditions: $[\text{Al}]_0:[\text{Zr}]_0 = 200:1$, 150 mg TiBA scavenger, 2 bar ethylene, 10 mg pre-catalyst, 50 mL hexanes and 30 minutes.

Solid MAO supported slurry-phase ethylene polymerisation

Slurry-phase ethylene polymerisation reactions were conducted in a 150 mL ampoule with 50 mL hexanes, 10 mg pre-catalyst, 150 mg triisobutylaluminium (TiBA) scavenger with a scavenger to aluminium ([Scav]₀: [Al]₀) ratio of 1000:1, 2 bar ethylene and an initial aluminium to metal ([Al]₀: [Zr]₀) loading of 200:1. All the polymerisation data are collated in Tables S3–S14.

Fig. 2a–4a show the slurry-phase ethylene polymerisation activity of the permethylindenyl complexes (**1–7**, **A** and **B**) supported on solid polymethylaluminoxane (sMAO), and Fig. 2b–4b show the corresponding molecular weights (M_w) of the polymers produced over the temperature range (50–90 °C). Fig. 2a and 3a show the ethylene polymerisation activity when the initiating groups are varied (X = Cl, Br, CH₂Ph, Me). For Me₂SB(Cp^R, I*)ZrX₂ (R = H, Me) at 80 °C polymerisation activity follows the series: X = Me > CH₂Ph > Cl > Br (**6**_{sMAO} > **4**_{sMAO} > **A**_{sMAO} > **2**_{sMAO} and **7**_{sMAO} > **5**_{sMAO} > **B**_{sMAO} > **3**_{sMAO}). This can be rationalised due to the decrease in electron density at the metal centre, stemming from the electron withdrawing and donating abilities of the initiating groups. Alkyl initiating groups possess an electron donating effect, while halides withdraw electron density from the metal centre. Lee *et al.* found that increasing the electron withdrawing ability of indenyl ligands led to a decrease in solution-phase ethylene polymerisation activity due to a decrease in propagation and chain-transfer rates.³⁷ The decrease in activity on moving from alkyl to halide initiation groups could also suggest that polymerisation activity is dependent on the efficiency of initiation group abstraction by the co-catalyst; recent results in the group show that generation of the active species via halide abstraction is less efficient than by alkyl abstraction.

Fig. 4a shows how the slurry-phase ethylene polymerisation activity varies as the Cp^R substituent is changed (R = H, Me, ⁿBu). Polymerisation activity decreases with increased steric hinderance around the metal centre, according to the series **E-1**_{sMAO} > **B**_{sMAO} > **A**_{sMAO} > **Z-1**_{sMAO}. The decrease in activity is most likely due to the increase in the relative size of the R substituent, with bulkier R groups inhibiting initial coordination of ethylene monomers to the metal centre. At 80 °C, **E-1**_{sMAO} is 30% more active than **Z-1**_{sMAO} under the same polymerisation conditions. This can be rationalised due to the additional steric hinderance provided by *n*-butyl chain when it is positioned directly below the I* ring, which obstructs the metal centre and prevents coordination of ethylene monomers. The improved polymerisation activity of **E-1** relative to **A** and **B** can be explained by the enhanced donor ability of *n*-butyl over methyl or hydrogen, which could provide additional stabilisation to the charged intermediates present in the polymerisation mechanism.

Across these ten pre-catalysts, the optimum activity is recorded for sMAO-Me₂SB(Cp^{Me}, I*)ZrMe₂ (**7**_{sMAO}) after 5 minutes of polymerisation at 80 °C at 2 bar ethylene (9509 kg_{PE} mol_M⁻¹ h⁻¹ bar⁻¹), the temperature at which these polymerisations are commonly conducted in industry. At a polymerisation time of 30 minutes at 80 °C, **7**_{sMAO} is 83% more active than an industrial

standard, sMAO supported (Cp^{nBu})₂ZrCl₂, under the same polymerisation conditions (6346 and 3459 kg_{PE} mol_{Zr}⁻¹ h⁻¹ bar⁻¹ respectively). At 60 °C after 30 minutes of polymerisation **7**_{sMAO} has an activity 59% higher than the previously reported ethylene bridged zirconocene sMAO-*rac*-(EBI*)ZrCl₂ under the same conditions (7948 and 5006 kg_{PE} mol_{Zr}⁻¹ h⁻¹ bar⁻¹ respectively) (Table 2).³⁰ Above 60 °C, the activity of **7**_{sMAO} decreases to afford an activity of 4382 kg_{PE} mol_{Zr}⁻¹ h⁻¹ bar⁻¹ at 90 °C (Fig 3a). A decrease in activity is observed for all ten sMAO supported complexes at 90 °C, suggesting either deactivation or decomposition at elevated temperature, or that polymerisation activity is affected by the decrease in the solubility of ethylene in hexane at higher temperatures.³⁸

Table 2 displays the slurry-phase ethylene polymerisation activity of a range of sMAO supported I* pre-catalysts and a known industrial complex. At 60 °C, after 30 minutes of polymerisation, “unsymmetrical” mono permethylindenyl catalyst sMAO-Me₂SB(Cp, I*)ZrCl₂ (**A**_{sMAO}) with [Al]₀: [Zr]₀ = 200:1 has an activity 18% greater than analogous “symmetrical” bis(permethylindenyl) zirconocene sMAO-*rac*-(SBI*)ZrCl₂ with [Al]₀: [Zr]₀ = 300:1 under the same conditions.³⁰ **A**_{sMAO} also shows an activity 52% higher than industrial standard sMAO-(Cp^{nBu})₂ZrCl₂ under identical polymerisation conditions and [Al]₀: [Zr]₀ loading. The very high slurry-phase ethylene activity of these unsymmetrical *ansa*-bridged I* complexes can be further confirmed by the comparison of sMAO-Me₂SB(Cp, I*)Zr(CH₂Ph)₂ (**4**_{sMAO}) and analogous sMAO-*meso*-(EBI*)Zr(CH₂Ph)₂, with [Al]₀: [Zr]₀ = 200:1 and 300:1 respectively; at 60 °C, **4**_{sMAO} is 21% more active than sMAO-*meso*-(EBI*)Zr(CH₂Ph)₂ under identical polymerisation conditions.³⁰ A plausible explanation for the large increase in polymerisation activity lies in the sterics of the system, with the decrease in the steric bulk of Cp^R compared to Ind* opening up the metal centre and allowing for easier coordination of ethylene monomers.

Polymer analysis

The molecular weights (M_w) of the polyethylenes produced were characterised by gel-permeation chromatography (GPC) (Fig. 2b–4b, S28). The molecular weights of the polyethylenes decrease with increasing temperature of polymerisation, this is attributed to stronger chain transfer reactions at higher temperatures³⁹ and an increase in the rate of termination relative to propagation (at elevated temperatures the system has more energy to overcome the higher activation barrier of termination).⁴⁰ The lowest molecular weights were recorded for **E-1**_{sMAO} and **7**_{sMAO} (M_w of 46 and 48 kg mol⁻¹ respectively at 80 °C). When compared to previously reported sMAO-*rac*-(SBI*)ZrCl₂ and sMAO-*meso*-(EBI*)Zr(CH₂Ph)₂, (M_w of 183 and 177 kg mol⁻¹ respectively) analogous **A**_{sMAO} and **4**_{sMAO} produce polyethylenes with molecular weights 23 and 27% lower respectively at 60 °C (140 and 130 kg mol⁻¹ respectively). This series of catalysts consistently produces polyethylenes with low molecular weights across the entire temperature range, with molecular weights almost half of that produced from industrial standard sMAO-(Cp^{nBu})₂ZrCl₂ at 80 °C (130 kg mol⁻¹). The polydispersity index (PDI = M_w/M_n) of the polymers

produced from the supported complexes falls within the range 2.7–4.2, with the narrowest PDI recorded for $\text{sMAO-Me}_2\text{SB}(\text{Cp}^{\text{Me}}, \text{I}^*)\text{ZrCl}_2$ (**B_{sMAO}**) (2.8 average across the temperature range). The M_w/M_n indicates the species to be largely single-site catalysts, and the resultant polymer to therefore be relatively homogeneous.

The homogeneity of the polymers can be further confirmed by scanning electron microscopy (SEM). SEM shows the sMAO supported complexes form polyethylene as discrete, “popcorn” shaped particles of uniform size and morphology; mimicking the morphology of the solid support (Fig. 5, S39–S48).⁴¹

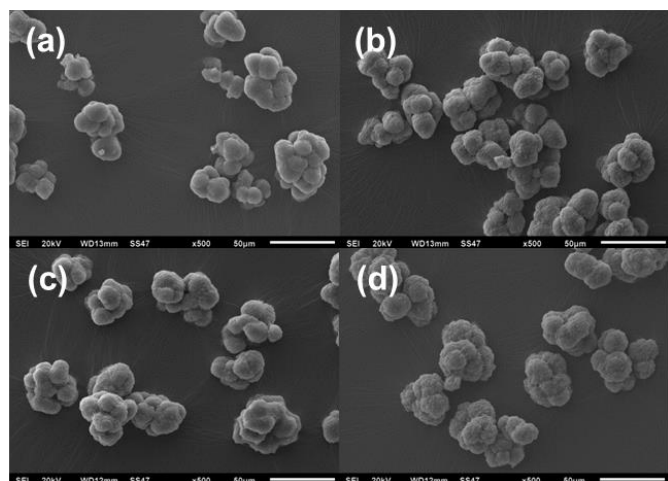


Fig. 5 Scanning electron microscopy images (SEM) of the polymers produced from: (a) **A_{sMAO}**, (b) **2_{sMAO}**, (c) **4_{sMAO}** and (d) **6_{sMAO}**. Polymerisation conditions: $[\text{Al}]_0:[\text{Zr}]_0 = 200:1$, 150 mg TiBA scavenger, 2 bar ethylene, 10 mg pre-catalyst, 50 mL hexane, 80 °C and 30 minutes.

Differential Scanning Calorimetry (DSC) analysis of the polyethylenes produced at 80 °C reveals a melting temperature (T_m) of 131–133 °C and crystallisation temperature (T_c) between 118 and 123 °C (Table S23, Fig. S31–33). A melting temperature of ~134 °C is indicative of HDPE with no defects or branching.^{41, 42} By integrating the areas under the peaks for T_m and T_c and dividing by the heating rate, the enthalpy of melting (ΔH_m) and crystallisation (ΔH_c) were calculated in the range 184–220 J g^{−1} and 174–212 J g^{−1} respectively. The recorded enthalpy of melting is much lower than that of 100% crystalline polyethylene (293 J g^{−1}),⁴³ and the percentage crystallinity of the polymer was calculated to be between 63 and 75%.

Conditions variation

All sMAO supported complexes show a similar trend in activity over time, with a decrease in activity observed at longer polymerisation time (displayed in Fig. S29 for $\text{sMAO-Me}_2\text{SB}(\text{Cp}, \text{I}^*)\text{ZrX}_2$ ($\text{X} = \text{Cl}, \text{Br}, \text{CH}_2\text{Ph}, \text{Me}$ at 80 °C). This is most likely due to decomposition of the catalyst, or due to a decrease in the rate of diffusion of monomer at longer polymerisation time, which leads to a decrease in the concentration of monomer present at the catalytic active site. This result is consistent with literature reports of other heterogeneous polymerisation systems.^{8,32,36,39,45, 32, 36, 39, 44} The molecular weights were also shown to decrease with time

(Fig. S30), most likely due an increase in number of termination steps relative to propagation at prolonged polymerisation time.

Varying the scavenger to aluminium ratio had interesting effects on the slurry-phase polymerisation activity (Fig. S34). For $\text{sMAO-Me}_2\text{SB}(\text{Cp}, \text{I}^*)\text{ZrCl}_2$ (**A_{sMAO}**), activity reached an optimum at a $[\text{Scav}]_0:[\text{Al}]_0$ ratio of 250:1 (5176 kg_{PE} mol_{Zr}^{−1} h^{−1} bar^{−1}); four times less TiBA scavenger than is used in our standard slurry-phase ethylene polymerisation set-up. However, for $\text{sMAO-Me}_2\text{SB}(\text{Cp}^{\text{Me}}, \text{I}^*)\text{Zr}(\text{CH}_2\text{Ph})_2$ (**5_{sMAO}**) the $[\text{Scav}]_0:[\text{Al}]_0$ ratio had little effect on activity, with activity ranging between 4601 and 5269 kg_{PE} mol_{Zr}^{−1} h^{−1} bar^{−1} across the range studied. These findings have an industrial impact, as the TiBA scavenger is a large industrial expense. It is of interest to note that when no scavenger is included in the polymerisation set-up, the activity tails off to 85 and 175 kg_{PE} mol_{Zr}^{−1} h^{−1} bar^{−1} for **A_{sMAO}** and **5_{sMAO}** respectively. The polymer morphology also changes from free-flowing, discrete, spherical particles to aggregated clumps.

The relative $[\text{Al}]_0:[\text{Zr}]_0$ loading of $\text{sMAO-Me}_2\text{SB}(\text{Cp}, \text{I}^*)\text{ZrCl}_2$ (**A_{sMAO}**), $\text{sMAO-Me}_2\text{SB}(\text{Cp}, \text{I}^*)\text{Zr}(\text{CH}_2\text{Ph})_2$ (**4_{sMAO}**) and $\text{sMAO-Me}_2\text{SB}(\text{Cp}, \text{I}^*)\text{ZrMe}_2$ (**6_{sMAO}**) was varied between 100:1 and 300:1 (Fig. S35). It was found that activity decreased as $[\text{Al}]_0:[\text{Zr}]_0$ loading decreased across the temperature range for all three pre-catalysts (from above 6000 to below 3500 kg_{PE} mol_{Zr}^{−1} h^{−1} bar^{−1}). This is perhaps counterintuitive as a lower loading equates to more zirconium sites immobilised onto the sMAO support. However, it is hypothesised that overloading of the solid support increases the number of inactive catalytic sites relative to active sites.

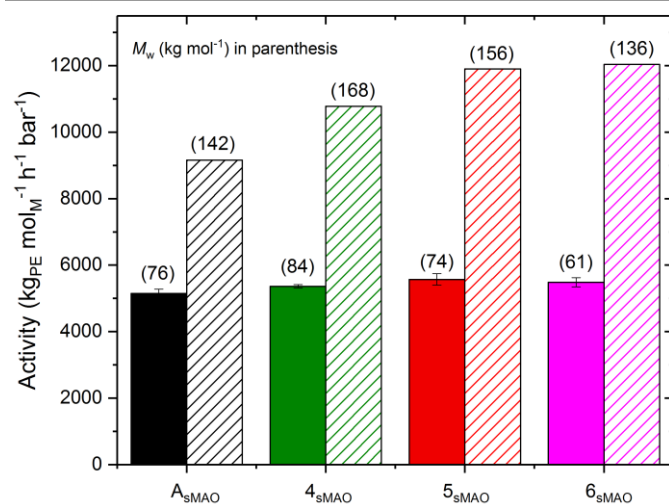


Fig. 6 Slurry-phase polymerisation activity and molecular weights, (M_w , in parenthesis) for $\text{sMAO-Me}_2\text{SB}(\text{Cp}, \text{I}^*)\text{ZrCl}_2$ (**A_{sMAO}**) (black), $\text{sMAO-Me}_2\text{SB}(\text{Cp}, \text{I}^*)\text{Zr}(\text{CH}_2\text{Ph})_2$ (**4_{sMAO}**) (green), $\text{sMAO-Me}_2\text{SB}(\text{Cp}^{\text{Me}}, \text{I}^*)\text{Zr}(\text{CH}_2\text{Ph})_2$ (**5_{sMAO}**) (red) and $\text{sMAO-Me}_2\text{SB}(\text{Cp}, \text{I}^*)\text{ZrMe}_2$ (**6_{sMAO}**) (pink). Standard scale polymerisation conditions (block colour): 150 mL reactor, $[\text{Al}]_0:[\text{Zr}]_0 = 200:1$, 150 mg TiBA scavenger, 2 bar ethylene, 10 mg pre-catalyst, 50 mL hexanes, 80 °C and 30 minutes. Large scale polymerisation conditions (patterned): 500 mL reactor, $[\text{Al}]_0:[\text{Zr}]_0 = 200:1$, 750 mg TiBA scavenger, 2 bar ethylene, 10 mg pre-catalyst, 250 mL hexanes, 80 °C and 30 minutes.

The effect of scale on polymerisation activity was also studied with the reactor vessel increased from 150 to 500 mL. **A_{sMAO}**, **4_{sMAO}**, **5_{sMAO}** and **6_{sMAO}** were studied in this larger polymerisation set-up. The solvent volume was increased from

50 to 250 mL hexanes, and the mass of the TiBA scavenger increased to 750 mg to account for this. The mass of pre-catalyst (10 mg) and ethylene pressure (2 bar) were kept constant, and the polymerisations conducted at 80 °C for 30 minutes. On a larger scale the trend in activity remained the same as on the smaller scale according to the series $6_{\text{sMAO}} > 5_{\text{sMAO}} > 4_{\text{sMAO}} > A_{\text{sMAO}}$ (Fig. 6). However, the activity approximately doubled for each supported complex (activity of 5482 and 12036 $\text{kg}_{\text{PE}} \text{mol}_{\text{Zr}}^{-1} \text{h}^{-1} \text{bar}^{-1}$ for 6_{sMAO} on the smaller and larger scale respectively). It is postulated that this large increase in activity is due to gas-liquid mass-transfer limitations on the smaller scale.

Analysis of the polymers produced from the larger scale system shows that the molecular weights approximately double when compared to the polymers produced from the smaller reaction vessel (an increase from 61 to 136 kg mol^{-1} for 6_{sMAO}). This shows that although the rate of polymerisation, and therefore activity, is higher on the larger scale, less termination steps occur relative to propagation. The SEM images of the polymer (Fig. S49-S51) show that solvent volume has little effect on the morphology of the polymer; however, the relative size of the individual particles increases by about 30% (from approximately 35 to 45 μm for the polymer produced from A_{sMAO} on the smaller and larger scale respectively).

Solid support variation

In order to study the effect of the support on slurry-phase ethylene polymerisation activity and polymer morphology, complexes **A**, **B**, **4** and **6** were immobilised onto three different inorganic supports; solid MAO (sMAO), MAO modified silica (SSMAO) and MAO modified $\text{Mg}_3\text{Al-CO}_3$ layered double hydroxide (LDHMAO), Fig. 7 and S36-38, and Tables 3 and S15-S22.

The sMAO supported complexes gave catalytic activities much higher than the analogous LDHMAO and SSMAO supported complexes over the temperature range (Fig. 7a,

S36-S38). A_{SSMAO} , B_{SSMAO} and 6_{SSMAO} consistently outperformed A_{LDHMAO} , B_{LDHMAO} and 6_{LDHMAO} , with a maximum activity of 1227 $\text{kg}_{\text{PE}} \text{mol}_{\text{M}}^{-1} \text{h}^{-1} \text{bar}^{-1}$ for 6_{SSMAO} at 80 °C. When compared to SSMAO-*rac*-(SBI*) ZrCl_2 at 70 °C (Table 3), A_{SSMAO} , 4_{SSMAO} and 6_{SSMAO} are 57, 62 and 84% more active respectively, however, B_{SSMAO} is 20% less active. Interestingly, 4_{LDHMAO} gave a consistently higher activity than 4_{SSMAO} , with a peak in activity at 80 °C (3182 $\text{kg}_{\text{PE}} \text{mol}_{\text{M}}^{-1} \text{h}^{-1} \text{bar}^{-1}$). At 80 °C, 4_{LDHMAO} is a very active LDHMAO pre-catalyst, with an activity 49% higher than LDHMAO supported $(\text{Cp}^{\text{nBu}})_2\text{ZrCl}_2$ under the same polymerisation conditions (activity of 2141 $\text{kg}_{\text{PE}} \text{mol}_{\text{M}}^{-1} \text{h}^{-1} \text{bar}^{-1}$ at 60 °C).³³ It is tentatively hypothesised that the large differences in activity observed between the three supports is due to the nature of the active species formed,^{32, 46} and the potential effects of non-innocent initiation groups.

The polymers produced from LDHMAO and SSMAO supported $\text{Me}_2\text{SB}(\text{Cp}, \text{I}^*)\text{Zr}(\text{CH}_2\text{Ph})_2$ (**4**) were analysed by GPC (Fig. 7b), which shows that 4_{sMAO} produces polymers with significantly lower molecular weights than 4_{SSMAO} and 4_{LDHMAO} across the temperature range (84, 316 and 252 kg mol^{-1} respectively at 80 °C). This is expected due to the much higher polymerisation activity of 4_{sMAO} . This could be attributed to stronger chain transfer reactions leading to an increase in the rate of termination relative to propagation (at elevated temperatures, the system has more energy to overcome the higher activation barrier of termination).^{33, 46} Therefore, decreasing the polymer molecular weight. The polymers produced from SSMAO and LDHMAO have fairly similar molecular weights, ranging from 251-699 kg mol^{-1} across the temperature range for 4_{SSMAO} and 228-603 kg mol^{-1} for 4_{LDHMAO} , with 4_{LDHMAO} consistently producing polymer with a lower molecular weight than 4_{SSMAO} . 4_{SSMAO} and 4_{LDHMAO} give polymers with much higher molecular weights than SSMAO-*rac*-(SBI*) ZrCl_2 and LDHMAO-*rac*-(SBI*) ZrCl_2 (262 and 277 kg mol^{-1} respectively at 70 °C),⁸ opposite to the effect seen when these complexes are supported on sMAO.

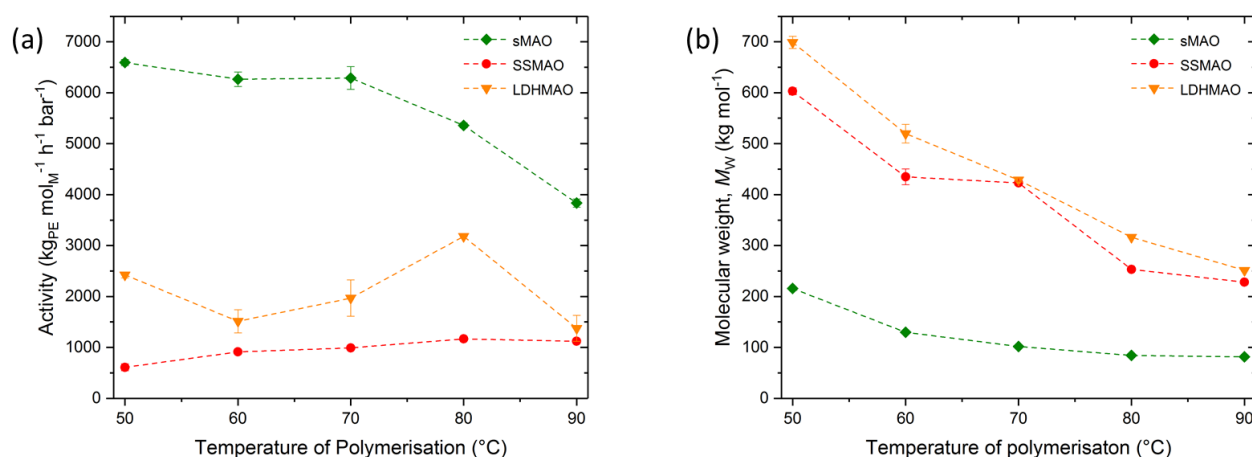


Fig 7. Ethylene polymerisation (a) activity and (b) molecular weights (M_w) as a function of temperature for $\text{Me}_2\text{SB}(\text{Cp}, \text{I}^*)\text{Zr}(\text{CH}_2\text{Ph})_2$ (**4**) supported on sMAO (4_{sMAO}) (green diamond), LDHMAO (orange down triangle) (4_{LDHMAO}) and SSMAO (4_{SSMAO}) (red circle). Polymerisation conditions: $[\text{Al}]_0: [\text{Zr}]_0 = 200:1$, 150 mg TiBA scavenger, 2 bar ethylene, 10 mg pre-catalyst, 50 mL hexanes and 30 minutes.

Table 3. Summary of the slurry-phase polymerisation of ethylene using selected methylaluminoxane modified silica (SSMAO) and methylaluminoxane modified layered double hydroxide (LDHMAO) supported I^* pre-catalysts.

Label	Catalyst	[Al] ₀ /[Zr] ₀	Temperature (°C)	Activity (kg _{PE} mol _{Zr} ⁻¹ h ⁻¹ bar ⁻¹)	M _w (kg mol ⁻¹)	M _w /M _n	Ref.
	SSMAO- <i>rac</i> -(EBI*)ZrCl ₂	200	70	2647	196	2.4	⁸
	SSMAO- <i>rac</i> -(SBI*)ZrCl ₂	200	70	611	262	3.2	⁸
	SSMAO-(^t Bu ₂ Flu, I*)ZrCl ₂	200	70	1015	698	2.6	^{41a}
A _{SSMAO}	SSMAO-Me ₂ SB(Cp, I*)ZrCl ₂	200	70	959	367	2.9	This work
B _{SSMAO}	SSMAO-Me ₂ SB(Cp ^{Me} , I*)ZrCl ₂	200	70	490	343	3.1	This work
4 _{SSMAO}	SSMAO-Me ₂ SB(Cp, I*)Zr(CH ₂ Ph) ₂	200	70	992	429	2.9	This work
6 _{SSMAO}	SSMAO-Me ₂ SB(Cp, I*)ZrMe ₂	200	70	1125	399	2.9	This work
	LDHMAO- <i>rac</i> -(EBI*)ZrCl ₂	200	70	4325	252	2.4	⁸
	LDHMAO-(^t Bu ₂ Flu, I*)ZrCl ₂	200	70	932	725	2.4	^{41a}
A _{LDHMAO}	LDHMAO-Me ₂ SB(Cp, I*)ZrCl ₂	200	70	80	-	-	This work
B _{LDHMAO}	LDHMAO-Me ₂ SB(Cp ^{Me} , I*)ZrCl ₂	200	70	254	-	-	This work
4 _{LDHMAO}	LDHMAO-Me ₂ SB(Cp, I*)Zr(CH ₂ Ph) ₂	200	70	1571	423	2.8	This work
6 _{LDHMAO}	LDHMAO-Me ₂ SB(Cp, I*)ZrMe ₂	200	70	967	-	-	This work

The SEM images of the polymers produced show that the industrially desirable mono-disperse polyethylene particles formed from sMAO supported complexes (Fig. 5) are replaced by larger, aggregated, poorly-defined polymer particles when the same complexes are supported on LDHMAO and SSMAO (Fig. 8, S53-S60).

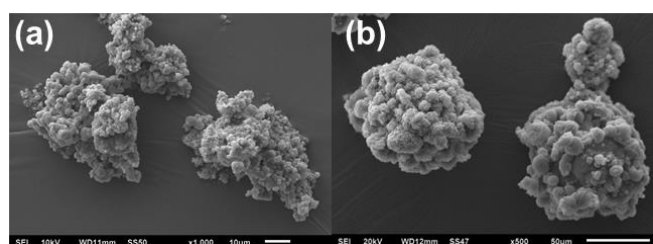


Fig. 8. Scanning electron microscopy images (SEM) of the polymers produced from: (a) 4_{LDHMAO} and (b) 4_{SSMAO}. Polymerisation conditions: [Al]₀/[Zr]₀ = 200:1, 150 mg TiBA scavenger, 2 bar ethylene, 10 mg pre-catalyst, 50 mL hexane, 80 °C and 30 minutes.

The drastic change in polymer morphology is attributed to the templating effect of the solid support, whereby the monomer enters the pores of the catalyst and polymer forms on the surface of the active sites.⁵ This effect influences the overall morphology of the polymer and has been seen in the literature with the B(C₆F₅)₃ modified sMAO support sMMAO(B(C₆F₅)₃). It has been shown that sMAO has a uniform “popcorn” morphology with particle size between 5 and 8 µm,³¹ while

LDHMAO has a poorly defined, aggregated “cauliflower” morphology, and SSMAO is composed of uniform, mono-disperse, granular particles about 10 µm in size (Fig. S61). The SEM images of the polymer clearly show that the characteristics of the support are replicated in the resultant polymer morphology.

Experimental

Synthesis of Me₂SB(CpⁿBu, I*)Li₂

1.0 equivalent LiCpⁿBu (1.52 g, 11.9 mmol) and 1.0 equivalent Ind*SiMe₂Cl (3.50 g, 11.9 mmol) were dissolved in THF (50 mL) in a Schlenk tube and stirred for 2 h. 2.2 equivalents ⁿBuLi (10.4 mL, 2.5 M in hexanes, 22.5 mmol) was added drop-wise at 0 °C, resulting in a colour change from dark orange to red, and the reaction mixture stirred for 1 h at 0 °C. The solvent was removed *in vacuo* and the resulting dark orange solid washed with pentane (3 × 50 mL) and diethyl ether (3 × 50 mL). The solid was dried to afford a brown powder (2.81 g) which was confirmed by ¹H NMR spectroscopy to be a 50:50 mixture of starting material and Me₂SB(CpⁿBu, I*)Li₂. Me₂SB(CpⁿBu, I*)Li₂ was therefore obtained in a 30% yield (1.41 g, 3.63 mmol). ¹H NMR (pyridine-*d*₅, 400 MHz, 23 °C) δ (ppm): 6.73 (CpH, 1H, m), 6.62 (CpH, 1H, m), 6.44 (CpH, 1H, m), 3.08 (ⁿBu, 2H, m), 3.06 (ArMe, 3H, s), 2.99 (ArMe, 3H, s), 2.95 (ArMe, 3H, s), 2.65 (ArMe, 3H,

s), 2.46 (ArMe, 3H, s), 2.30 (ArMe, 3H, s), 1.59 (ⁿBu, 2H, m), 1.48 (ⁿBu, 2H, m), 0.97 (SiMe, 6H, s), 0.78 (ⁿBu, 3H, m).

Synthesis of Me₂SB(CpⁿBu, I*)ZrCl₂ (1)

1.0 equivalent Me₂SB(CpⁿBu, I*)Li₂ (1.93 g, 4.96 mmol) and 1.0 equivalent ZrCl₄ (1.16 g, 4.96 mmol) were dissolved in benzene (50 mL) in a Schlenk tube and stirred for 16 h. The resulting dark red solution was filtered, the solvent removed and the product extracted with pentane (3 × 50 mL). Storage at –80 °C yielded an orange crystalline solid and through a series of pentane washes *E*-Me₂SB(CpⁿBu, I*)ZrCl₂ and *Z*-Me₂SB(CpⁿBu, I*)ZrCl₂ were isolated in 0.5% (13 mg, 0.02 mmol) and 0.9% (25 mg, 0.05 mmol) yield respectively. Crystals of *Z*-Me₂SB(CpⁿBu, I*)ZrCl₂, suitable for a single crystal X-ray diffraction study, were grown from a pentane solution at –34 °C. *E*-Isomer: ¹H NMR (benzene-*d*₆, 500 MHz, 23 °C) δ (ppm): 6.40 (CpH, 1H, m), 5.70 (CpH, 1H, m), 5.32 (CpH, 1H, m), 2.73 (ⁿBu, 2H, m), 2.62 (ArMe, 3H, s), 2.57 (ArMe, 3H, s), 2.29 (ArMe, 3H, s), 2.18 (ArMe, 3H, s), 2.06 (ArMe, 3H, s), 1.96 (ArMe, 3H, s), 1.48 (ⁿBu, 2H, m), 1.25 (ⁿBu, 2H, q, ³J_{HH} = 8 Hz), 0.81 (ⁿBu, 3H, t, ³J_{HH} = 8 Hz), 0.71 (SiMe, 3H, s), 0.61 (SiMe, 3H, s). ¹³C{¹H} NMR (benzene-*d*₆, 100 MHz, 23 °C) δ (ppm): 2.7 (SiMe), 5.0 (SiMe), 13.8 (CH₂Me), 15.5 (ArMe), 16.4 (ArMe), 16.7 (ArMe), 17.2 (ArMe), 17.5 (ArMe), 21.2 (ArMe), 22.6 (CH₂), 29.8 (CH₂), 32.4 (CH₂), 82.4 (ArSi), 104.5 (CpSi), 115.5 (CpH), 115.7 (CpH), 124.9 (CpH), 130.4 (Ar), 131.0 (Ar), 132.4 (Ar), 134.1 (Ar), 134.4 (Ar), 135.0 (Ar), 141.1 (CpⁿBu), 2 quaternary Ar missing. *Z*-Isomer: ¹H NMR (benzene-*d*₆, 500 MHz, 23 °C) δ (ppm): 6.43 (CpH, 1H, m), 5.62 (CpH, 1H, m), 5.59 (CpH, 1H, m), 2.61 (ArMe, 3H, s), 2.28 (ⁿBu, 2H, m), 2.56 (ArMe, 3H, s), 2.26 (ArMe, 3H, s), 2.16 (ArMe, 3H, s), 2.06 (ArMe, 3H, s), 2.02 (ArMe, 3H, s), 1.41 (ⁿBu, 2H, m), 0.87 (ⁿBu, 2H, t, ³J_{HH} = 8 Hz), 0.78 (ⁿBu, 3H, t, ³J_{HH} = 8 Hz), 0.69 (SiMe, 3H, s), 0.61 (SiMe, 3H, s). ¹³C{¹H} NMR (benzene-*d*₆, 100 MHz, 23 °C) δ (ppm): 141.9 (CpⁿBu), 136.0 (Ar), 134.5 (Ar), 134.1 (Ar), 132.9 (Ar), 130.8 (Ar), 124.8 (CpH), 117.1 (CpH), 115.6 (CpH), 105.0 (CpSi), 83.2 (ArSi), 32.1 (CH₂), 29.9 (CH₂), 22.9 (CH₂), 21.6 (CH₂Me), 17.8 (ArMe), 17.4 (ArMe), 17.1 (ArMe), 16.7 (ArMe), 15.7 (ArMe), 14.1 (ArMe), 5.2 (SiMe), 3.0 (SiMe), 3 quaternary Ar missing. CCDC number: 1883429 (*E*-) and 1883430 (*Z*-).

Synthesis of Me₂SB(Cp, I*)ZrBr₂ (2)

1.0 equivalent Me₂SB(Cp, I*)Li₂ (1.00 g, 3.00 mmol) and 1.0 equivalent ZrBr₄ (1.23 g, 3.00 mmol) were dissolved in benzene (50 mL) in a Schlenk tube and stirred for 18 h. The resulting dark orange solution was filtered, the solvent removed and the product extracted with pentane (3 × 50 mL). The insoluble redish powder was shown to be the desired product in 9% yield (154 mg, 0.27 mmol). Storage of the pentane solution at –34 °C yielded Me₂SB(Cp, I*)ZrBr₂ as red crystals in 6% yield (97 mg, 0.17 mmol). Single crystals suitable for X-ray diffraction study were obtained from a benzene solution at 5 °C. ¹H NMR (benzene-*d*₆, 500 MHz, 23 °C) δ (ppm): 6.81 (CpH, 1H, m), 6.77 (CpH, 1H, m), 5.63 (CpH, 1H, m), 5.35 (CpH, 1H, m), 2.62 (ArMe, 6H, s), 2.20 (ArMe, 3H, s), 2.14 (ArMe, 3H, s), 2.03 (ArMe, 3H, s), 1.86 (ArMe, 3H, s), 0.59 (SiMe, 3H, s), 0.53 (SiMe, 3H, s). ¹³C{¹H} NMR (benzene-*d*₆, 100 MHz, 23 °C) δ (ppm): 135.4 (Ar),

135.1 (Ar), 134.4 (Ar), 133.8 (Ar), 131.9 (Ar), 130.6 (Ar), 130.2 (Ar), 129.1 (Ar), 127.3 (CpH), 124.2 (CpH), 116.2 (CpH), 114.5 (CpH), 104.8 (CpSi), 82.5 (ArSi), 34.5 (ArMe), 21.2 (ArMe), 17.9 (ArMe), 17.4 (ArMe), 17.3 (ArMe), 16.8 (ArMe, ArMe), 5.1 (SiMe), 3.0 (SiMe). CHN Analysis (%): expected C 46.23, H 4.94, observed C 46.27, H 5.12. MS (EI): expected m/z = 567.94, observed m/z = 567.94. CCDC number: 1883431.

Synthesis of Me₂SB(Cp^{Me}, I*)ZrBr₂ (3)

1.0 equivalent Me₂SB(Cp^{Me}, I*)Li₂ (1.00 g, 2.87 mmol) and 1.0 equivalent ZrBr₄ (1.18 g, 2.88 mmol) were dissolved in benzene (50 mL) in a Schlenk tube and stirred for 18 h. The resulting dark orange solution was filtered, the solvent removed and the product extracted with pentane (3 × 50 mL). Storage at –80 °C yielded an isomeric mixture of Me₂SB(Cp^{Me}, I*)ZrBr₂ as an orange solid in 5% yield (84 mg, 1.38 mmol). *Isomer A*: ¹H NMR (benzene-*d*₆, 400 MHz, 23 °C) δ (ppm): 6.54 (CpH, 1H, m), 5.45 (CpH, 1H, m), 5.39 (CpH, 1H, m), 2.65 (ArMe, 3H, s), 2.63 (ArMe, 3H, s), 2.24 (ArMe, 3H, s), 2.17 (ArMe, 3H, s), 2.13 (CpMe, 3H, s), 2.03 (ArMe, 3H, s), 1.93 (ArMe, 3H, s), 0.61 (SiMe, 3H, s), 0.58 (SiMe, 3H, s). ¹³C{¹H} NMR (benzene-*d*₆, 100 MHz, 23 °C) δ (ppm): 135.5 (Ar), 134.9 (Ar), 134.6 (Ar), 134.4 (Ar), 134.2 (Ar), 131.9 (Ar), 130.0 (Ar), 129.9 (Ar), 129.2 (CpMe), 128.8 (CpH), 119.0 (CpH), 115.2 (CpH), 104.4 (CpSi), 82.2 (ArSi), 21.2 (CpMe), 17.9 (ArMe), 17.5 (ArMe), 17.4 (ArMe), 16.7 (ArMe, ArMe), 16.3 (ArMe), 4.7 (SiMe), 3.2 (SiMe), 1 quaternary carbon missing. *Isomer B*: ¹H NMR (benzene-*d*₆, 400 MHz, 23 °C) δ (ppm): 6.46 (CpH, 1H, m), 5.69 (CpH, 1H, m), 5.08 (CpH, 1H, m), 2.61 (ArMe, 6H, s), 2.28 (ArCMe, 3H, s), 2.21 (ArMe, 3H, s), 2.19 (CpMe, 3H, s), 2.03 (ArMe, 3H, s), 1.87 (ArMe, 3H, s), 0.64 (SiMe, 3H, s), 0.55 (SiMe, 3H, s). ¹³C{¹H} NMR (benzene-*d*₆, 100 MHz, 23 °C) δ (ppm): 136.6 (Ar), 135.2 (Ar), 135.1 (Ar), 134.8 (Ar), 133.5 (Ar), 131.8 (Ar), 130.6 (Ar), 129.1 (Ar), 129.1 (CpMe), 126.0 (CpH), 116.9 (CpH), 116.5 (CpH), 103.9 (CpSi), 81.8 (ArSi), 21.4 (CpMe), 18.0 (ArMe), 17.4 (ArMe), 17.4 (ArMe), 16.8 (ArMe), 16.8 (ArMe), 16.5 (ArMe), 5.1 (SiMe), 3.0 (SiMe). *Isomeric Mixture*: CHN Analysis (%): expected C 47.17, H 5.16, observed C 47.26, H 5.31.

Synthesis of Me₂SB(Cp, I*)Zr(CH₂Ph)₂ (4)

1.0 equivalent Me₂SB(Cp, I*)ZrCl₂ (0.19 g, 0.38 mmol) and 2.0 equivalents K(CH₂Ph) (0.10 g, 0.77 mmol) were added to a Schlenk tube, dissolved in benzene (10 mL) and stirred for 4 h. Filtration and removal of solvent *in vacuo* yielded Me₂SB(Cp, I*)Zr(CH₂Ph)₂ as a yellow solid in 44% yield (0.10 g, 0.17 mmol). Yellow crystals, suitable for a single crystal X-ray diffraction study, were obtained from a saturated pentane solution. ¹H NMR (benzene-*d*₆, 400 MHz, 23 °C) δ (ppm): 7.24 (*o*-Ph, 2H, m), 7.13 (*m*-Ph, *p*-Ph, 3H, m), 6.91 (*m*-Ph, *p*-Ph, 3H, m), 6.54 (*o*-Ph, 2H, m), 6.28 (CpH, 1H, m), 6.10 (CpH, 1H, m), 5.12 (CpH, 1H, m), 5.04 (CpH, 1H, m), 2.52 (ArMe, 3H, s), 2.30 (ArMe, 3H, s), 2.23 (ArMe, 3H, s), 2.10 (ArMe, 6H, s), 1.81 (ArMe, 3H, s), 1.83 (PhCH, 1H, d, ³J_{H-H} = 12 Hz), 1.62 (PhCH, 1H, d, ³J_{H-H} = 12 Hz), 0.56 (SiMe, 3H, s), 0.53 (SiMe, 3H, s), 0.33 (PhCH, 1H, d, ³J_{H-H} = 12 Hz), 0.05 (PhCH, 1H, d, ³J_{H-H} = 12 Hz). ¹³C{¹H} NMR (benzene-*d*₆, 100 MHz, 23 °C) δ (ppm): 153.9 (PhCH₂), 153.5 (PhCH₂), 133.5 (Ar), 133.4 (Ar), 133.2 (Ar), 130.8 (Ar), 130.0 (Ar),

129.1 (Ph), 128.3 (Ar), 128.2 (Ph), 128.0 (Ph), 127.7 (Ph), 126.4 (Cp), 126.2 (Ph), 125.5 (Ar), 124.6 (Ph), 121.9 (Ar), 121.0 (Ph), 120.8 (Ph), 119.3 (Cp), 118.7 (Cp), 113.0 (Cp), 100.6 (CpSi), 77.1 (ArSi), 67.9 (PhCH₂), 61.3 (PhCH₂), 21.4 (ArMe), 21.2 (ArMe), 17.1 (ArMe), 16.4 (ArMe), 16.2 (ArMe), 14.4 (ArMe), 4.2 (SiMe), 3.0 (SiMe). ²⁹Si NMR (benzene-*d*₆, 100 MHz, 298 K) δ (ppm): -15.45 (SiMe). CHN Analysis (%): expected C 72.79, H 7.13, observed C 72.34, H 6.89. MS (EI): molecular ion not found, major ^{Me}SB(Cp,I*)Zr(CH₂Ph)⁺ fragment observed at 501.154. IR (KBr) (cm⁻¹): 3061, 3007, 2905 (b), 1572, 1481, 1374 (b), 1254, 1208, 983, 821 (b), 746, 697, 673. CCDC number: 1883432.

Synthesis of ^{Me}SB(Cp^{Me},I*)Zr(CH₂Ph)₂ (5)

1.0 equivalent ^{Me}SB(Cp^{Me},I*)ZrCl₂ (50 mg, 0.10 mmol) and 2.4 equivalents K(CH₂Ph) (31.5 mg, 0.24 mmol) were added to a Young's tap NMR tube. Benzene-*d*₆ (0.5 mL) was added and the solution heated at 70 °C for 60 h. Filtration on a frit and removal of solvent *in vacuo* yielded ^{Me}SB(Cp^{Me},I*)Zr(CH₂Ph)₂ as an orange oil which was freeze dried in benzene to give a yellow solid in 78% yield (48 mg, 0.08 mmol). *Isomer A*: ¹H NMR (benzene-*d*₆, 400 MHz, 23 °C) δ (ppm): 7.24–6.60 (Ph, 10H, m), 5.84 (CpH, 1H, m), 5.26 (CpH, 1H, m), 5.12 (CpH, 1H, m), 2.57 (ArMe, 3H, s), 2.47 (ArMe, 3H, s), 2.27 (ArMe, 3H, s), 2.11 (ArMe, 3H, s), 2.07 (ArMe, 3H, s), 1.99 (PhCH, 1H, d, ³J_{H-H} = 12 Hz), 1.82 (ArMe, 3H, s), 1.79 (CpMe, 3H, s), 1.79 (PhCH, 1H, d, ³J_{H-H} = 12 Hz), 1.68 (PhCH, 1H, d, ³J_{H-H} = 8 Hz), 0.72 (PhCH, 1H, d, ³J_{H-H} = 12 Hz), 0.63 (SiMe, 3H, s), 0.53 (SiMe, 3H, s), -0.01 (PhCH, 1H, d, ³J_{H-H} = 8 Hz). ¹³C{¹H} NMR (benzene-*d*₆, 100 MHz, 23 °C) δ (ppm): 154.0 (PhCH₂), 151.5 (PhCH₂), 133.3 (CpMe), 123.0 (Cp), 116.7 (Cp), 115.5 (Cp), 100.7 (CpSi), 79.3 (ArSi), 67.7 (PhCH₂), 63.7 (PhCH₂), 21.8 (ArMe), 21.8 (CpMe), 17.3 (ArMe), 17.6 (ArMe), 16.5 (ArMe), 16.4 (ArMe), 14.7 (ArMe), 2.2 (SiMe), 3.4 (SiMe). Resonances between 128.6–121.0 (Ph) and 120.7–136.4 (Ar) cannot be further assigned. *Isomer B*: ¹H NMR (benzene-*d*₆, 400 MHz, 23 °C) δ (ppm): 7.24–6.60 (Ph, 10H, m), 6.17 (CpH, 1H, m), 5.37 (CpH, 1H, m), 5.06 (CpH, 1H, m), 2.29 (ArMe, 3H, s), 2.28 (ArMe, 3H, s), 2.25 (ArMe, 3H, s), 2.19 (PhCH, 1H, d, ³J_{H-H} = 8 Hz), 2.09 (ArMe, 3H, s), 2.03 (ArMe, 3H, s), 1.88 (ArMe, 3H, s), 1.57 (CpMe, 3H, s), 1.43 (PhCH, 1H, d, ³J_{H-H} = 12 Hz), 0.68 (PhCH, 1H, d, ³J_{H-H} = 12 Hz), 0.63 (SiMe, 3H, s), 0.53 (SiMe, 3H, s), 0.08 (PhCH, 1H, d, ³J_{H-H} = 8 Hz). ¹³C{¹H} NMR (benzene-*d*₆, 100 MHz, 23 °C) δ (ppm): 154.0 (PhCH₂), 151.0 (PhCH₂), 130.0 (CpMe), 126.7 (Cp), 120.7 (Cp), 113.4 (Cp), 100.5 (CpSi), 78.3 (ArSi), 65.7 (PhCH₂), 60.2 (PhCH₂), 21.7 (ArMe), 17.7 (ArMe), 17.2 (ArMe), 13.4 (CpMe), 15.0 (ArMe), 14.7 (ArMe), 14.4 (ArMe), 3.6 (SiMe), 3.2 (SiMe). Resonances between 128.6–121.0 (Ph) and 120.7–136.4 (Ar) cannot be further assigned. *Isomeric Mixture*: CHN Analysis (%): expected C 73.09, H 7.29, observed C 72.92, H 7.20. IR (KBr) (cm⁻¹): 2945 (b), 1596, 1480, 1450, 1378 (b), 1096 (b), 1030 (b), 845, 805, 742, 700.

Synthesis of ^{Me}SB(Cp,I*)ZrMe₂ (6)

1.0 equivalent ^{Me}SB(Cp,I*)ZrCl₂ (0.20 g, 0.41 mmol) was dissolved in toluene in a Schlenk tube and cooled to -78 °C. 2.2 equivalents MeLi (0.57 mL, 0.92 mmol, 1.6 M in diethyl ether) were added dropwise and the solution stirred for 4 h, resulting

in a colour change from orange to yellow. Filtration and removal of solvent *in vacuo* yielded ^{Me}SB(Cp,I*)ZrMe₂ as a yellow solid in 18% yield (33 mg, 0.17 mmol). ¹H NMR (benzene-*d*₆, 400 MHz, 23 °C) δ (ppm): 6.62 (CpH, 1H, m), 6.55 (CpH, 1H, m), 5.59 (CpH, 1H, m), 5.18 (CpH, 1H, m), 2.54 (ArMe, 3H, s), 2.44 (ArMe, 3H, s), 2.18 (ArMe, 6H, s), 2.08 (ArMe, 3H, s), 1.83 (ArMe, 3H, s), 0.63 (SiMe, 3H, s), 0.58 (SiMe, 3H, s), -0.11 (ZrMe, 3H, s), -1.18 (ZrMe, 3H, s). ¹³C{¹H} NMR (benzene-*d*₆, 100 MHz, 23 °C) δ (ppm): 132.0 (Ar), 131.7 (Ar), 131.4 (Ar), 131.2 (Ar), 129.4 (Ar), 129.1 (Ar), 126.9 (Ar), 121.0 (CpH), 119.9 (Ar), 117.8 (CpH), 114.4 (CpH), 111.6 (CpH), 99.4 (CpSi), 78.1 (ArSi), 33.5 (ZrMe), 31.7 (ZrMe), 21.0 (ArMe), 17.2 (ArMe), 17.0 (ArMe), 16.3 (ArMe), 16.1 (ArMe), 14.6 (ArMe), 5.1 (SiMe), 3.3 (SiMe). ²⁹Si NMR (benzene-*d*₆, 100 MHz, 298 K) δ (ppm): -16.28 (SiMe). MS (EI): molecular ion not found, major ^{Me}SB(Cp,I*)ZrMe⁺ fragment observed at 425.12. IR (KBr) (cm⁻¹): 2982, 2911, 2854, 1453 (b), 1381 (b), 1287, 1252, 1168, 1051, 839, 808, 677. CCDC number: 1883433.

Synthesis of ^{Me}SB(Cp^{Me},I*)ZrMe₂ (7)

1.0 equivalent ^{Me}SB(Cp^{Me},I*)ZrCl₂ (150 mg, 0.30 mmol) was dissolved in toluene in a Schlenk tube and cooled to -78 °C. 2.2 equivalents MeLi (0.42 mL, 0.60 mmol, 1.6 M in diethyl ether) were added dropwise and the solution stirred for 4 h, resulting in a colour change from orange to yellow. Filtration and removal of solvent *in vacuo* yielded ^{Me}SB(Cp^{Me},I*)ZrMe₂ as a dark orange oil which was freeze dried in benzene to give a yellow solid in 72% yield (99 mg, 0.22 mmol). *Isomer A*: ¹H NMR (benzene-*d*₆, 400 MHz, 23 °C) δ (ppm): 6.24 (CpH, 1H, m), 5.57 (CpH, 1H, m), 4.87 (CpH, 1H, m), 2.46 (ArMe, 6H, s), 2.21 (CpMe, 3H, s), 2.17 (ArMe, 3H, s), 2.10 (ArMe, 6H, s), 1.81 (ArMe, 3H, s), 0.65 (SiMe, 3H, s), 0.60 (SiMe, 3H, s), -0.24 (ZrMe, 3H, s), -1.19 (ZrMe, 3H, s). ¹³C{¹H} NMR (benzene-*d*₆, 400 MHz, 23 °C) δ (ppm): 132.2 (Ar), 131.9 (Ar), 131.7 (Ar), 131.2 (Ar), 129.6 (Ar), 129.5 (Ar), 127.5 (Ar), 127.0 (Ar), 120.0 (CpMe), 118.2 (CpH), 115.3 (CpH), 112.5 (CpH), 99.2 (CpSi), 77.7 (ArSi), 36.6 (ZrMe), 33.0 (ZrMe), 21.3 (CpMe), 17.5 (ArMe), 17.2 (ArMe), 16.5 (ArMe), 16.4 (ArMe), 14.9 (ArMe, ArMe), 5.1 (SiMe), 3.5 (SiMe). *Isomer B*: ¹H NMR (benzene-*d*₆, 400 MHz, 23 °C) δ (ppm): -1.28 (ZrMe, 3H, s), -0.14 (ZrMe, 3H, s), 0.61 (SiMe, 3H, s), 0.62 (SiMe, 3H, s), 1.89 (ArMe, 3H, s), 2.11 (ArMe, 6H, s), 2.13 (CpMe, 3H, s), 2.19 (ArMe, 3H, s), 2.58 (ArMe, 6H, s), 5.14 (CpH, 1H, m), 5.40 (CpH, 1H, m), 6.33 (CpH, 1H, m). ¹³C{¹H} NMR (benzene-*d*₆, 100 MHz, 23 °C) δ (ppm): 132.3 (Ar), 132.2 (Ar), 131.8 (Ar), 131.2 (Ar), 130.6 (CpMe), 129.6 (Ar), 129.5 (Ar), 128.6 (Ar), 126.9 (Ar), 122.0 (CpH), 116.2 (CpH), 112.3 (CpH), 99.0 (CpSi), 78.3 (ArSi), 35.6 (ZrMe), 30.2 (ZrMe), 21.3 (CpMe), 17.5 (ArMe), 17.2 (ArMe), 16.5 (ArMe), 16.5 (ArMe), 15.0 (ArMe, ArMe), 5.0 (SiMe), 3.6 (SiMe).

Synthesis of the activated supports (SSMAO, LDHMAO)

Toluene (40 mL) was added to 1.0 equivalent SiO₂ or LDH (Mg₃Al-CO₃) and 0.5 equivalents MAO in a Schlenk tube and the mixture heated at 80 °C for 2 h with swirling. The colourless solid was allowed to settle, the solution decanted and the product dried under vacuum to give the activated supports in quantitative yield.

Synthesis of supported catalysts

The activated support and complex were weighed into a Schlenk tube. Toluene (40 mL) was added and the solution heated at 60 °C for 1 h with swirling. The coloured solid was allowed to settle and the clear, colourless supernatant decanted. The solid was dried *in vacuo* to give the product as a faintly coloured powder in quantitative yield.

sMAO-Me₂SB(Cp,ⁱ*)ZrCl₂ (A_{sMAO}): ²⁹Si CPMAS NMR (10 kHz, 23 °C) δ (ppm): -12.2, -168.2. ¹³C CPMAS NMR (10 kHz, 23 °C) δ (ppm): 137.5, 135.2, 131.6, 128.5, 25.1, 20.4, 18.9, 17.1, 16.1, -7.9 (AlOMe). ²⁷Al DPMAS NMR (15 kHz, 23 °C) δ (ppm): 347.1, 208.8, 82.6, -83.1, -240.8. IR (KBr) (cm⁻¹): 2948 (b), 1593, 1536, 1272, 732 (b).

sMAO-Me₂SB(Cp^{Me},ⁱ*)ZrCl₂ (B_{sMAO}): IR (KBr) (cm⁻¹): 3025, 2951 (b), 1598, 1540, 1445, 1367, 1219, 756 (b).

sMAO-Me₂SB(Cp,ⁱ*)Zr(CH₂Ph)₂ (4_{sMAO}): ²⁹Si CPMAS NMR (10 kHz, 23 °C) δ (ppm): -12.1. ¹³C CPMAS NMR (10 kHz, 23 °C) δ (ppm): 137.1, 131.2, 128.2, 125.4, 32.6, 26.8, 23.1, 19.4, 15.3, -7.6 (AlOMe). ²⁷Al DPMAS NMR (15 kHz, 23 °C) δ (ppm): 343.5, 204.5, 82.5, -83.1, -238.8. IR (KBr) (cm⁻¹): 2953 (b), 1598, 1534, 1449, 1382, 753 (b).

sMAO-Me₂SB(Cp,ⁱ*)ZrMe₂ (6_{sMAO}): ²⁹Si CPMAS NMR (10 kHz, 23 °C) δ (ppm): -13.9. ¹³C CPMAS NMR (10 kHz, 23 °C) δ (ppm): 136.0, 131.1, 128.7, 125.4, 51.7, 20.3, 16.4, -7.7 (AlOMe). ²⁷Al DPMAS NMR (15 kHz, 23 °C) δ (ppm): 346.5, 208.2, 76.6, -82.9, -241.6. IR (KBr) (cm⁻¹): 2951 (b), 1508, 1446, 1217, 742 (b).

Slurry-phase ethylene polymerisation

TiBA (150 mg) in hexane (10 mL) was added to a 150 mL Rotafluo ampoule. The supported complex (10 mg) was added and washed with hexane (40 mL). The ampoule headspace was degassed whilst heating to temperature. The ampoule was opened to ethylene gas (2 bar) and the solution stirred at 1000 rpm for the duration of the run. On completion, the reaction mixture was degassed and the polymer filtered, washed with pentane (2 × 25 mL) and dried under reduced pressure on a frit. All runs were carried out, at least, in duplicate.

Conclusions

Ten permethylindenyl zirconocene complexes of the type Me₂(Cp^R,ⁱ*)ZrX₂ have been synthesised and fully characterised. The complexes were successfully immobilised on three inorganic solid supports (sMAO, LDHMAO and SSMAO) and the slurry-phase ethylene polymerisation activity studied under various conditions.

sMAO supported Me₂SB(Cp^{Me},ⁱ*)ZrMe₂ displays the highest ethylene polymerisation activity (9509 kg_{PE} mol_M⁻¹ h⁻¹ bar⁻¹ at 80 °C in 50 mL hexane after 5 minutes with 2 bar ethylene). After 30 minutes of polymerisation Me₂SB(Cp^{Me},ⁱ*)ZrMe₂ is 85% more active than an industrial standard, sMAO supported (n^{Bu}Cp)₂ZrCl₂ under the same polymerisation conditions (6346 and 3459 mol_{Zr}⁻¹ h⁻¹ bar⁻¹ respectively). These catalytic systems produce polyethylenes with low molecular weights (*M*_w of 46 kg mol⁻¹ for sMAO-E-Me₂SB(Cp^{nBu},ⁱ*)ZrCl₂ at 90 °C).

It was established that solvent volume plays a huge role in polymerisation activity and molecular weight of the polymer produced, with activity and molecular weight approximately doubling with a 5-fold increase in solvent. Upon support variation it was found that LDHMAO supported Me₂SB(Cp,ⁱ*)Zr(CH₂Ph)₂ is one of the most active LDHMAO supported zirconocenes to date with a maximum activity of 3182 kg_{PE} mol⁻¹ h⁻¹ bar⁻¹ at 80 °C. SEM imaging of the polyethylene produced showed that sMAO supported complexes give polyethylene with a much more uniform, mono-disperse and industrially desirable morphology than the same species supported on LDHMAO and SSMAO.

Acknowledgements

J.V.L., J.-C.B. and Z.R.T. (for SCG Research Fellowship) would like to thank SCG Chemicals Co., Ltd. (Thailand) for financial support, Dr. Nicholas H. Rees (University of Oxford) for solid state NMR spectroscopy experiments, Chemical Crystallography (University of Oxford) for the use of the diffractometers, Research Complex at Harwell for use of the Scanning Electron Microscope, Ms Liv Thobru (Norner AS, Norway) for GPC, and Prof. Charlotte Williams (University of Oxford) for use of the Differential Scanning Calorimeter.

Notes and references

- 1 L. Resconi, L. Cavallo, A. Fait and F. Piemontesi, *Chem. Rev.*, 2000, **100**, 1253-1346.
- 2 G. G. Hlatky, *Chem. Rev.*, 2000, **100**, 1347-1376.
- 3 W. Kaminsky, A. Funck and H. Haehnsen, *Dalton Trans.*, 2009, 8803-8810.
- 4 G. W. Coates, *Chem. Rev.*, 2000, **100**, 1223-1252.
- 5 J. R. Severn, J. C. Chadwick, R. Duchateau and N. Friederichs, *Chem. Rev.*, 2005, **105**, 4073-4147.
- 6 P. A. Zapata, C. Belver, R. Quijada, P. Aranda and E. Ruiz-Hitzky, *App. Catal. A Gen.*, 2013, **453**, 142-150.
- 7 P. Wongwaiwattanukul and B. Jongsomjit, *Catal. Comm.*, 2008, **10**, 118-122.
- 8 J.-C. Buffet, T. A. Q. Arnold, Z. R. Turner, P. Angpanitcharoen and D. O'Hare, *RSC Adv.*, 2015, **5**, 87456-87464.
- 9 M. Sacchetti, S. Pasquali and G. Govoni, US5698487, 1997.
- 10 S. I. Woo and Y. S. Ko, US5869417, 1999.
- 11 H. G. Alt and A. Koppl, *Chem. Rev.*, 2000, **100**, 1205-1221.
- 12 P. Ransom, A. E. Ashley, N. D. Brown, A. L. Thompson and D. O'Hare, *Organometallics*, 2011, **30**, 800-814.
- 13 T. A. Q. Arnold, J.-C. Buffet, Z. R. Turner and D. O'Hare, *J. Organomet. Chem.*, 2015, **792**, 55-65.
- 14 P. J. Shapiro, *Coord. Chem. Rev.*, 2002, **231**, 67-81.
- 15 M. E. M. Abdelbagi, W. Milius, S. Mondal, S. van Smaalen and H. G. Alt, *J. Organomet. Chem.*, 2018, **854**, 76-86.
- 16 B. Wang, *Coord. Chem. Rev.*, 2006, **250**, 242-258.
- 17 A. S. Rodrigues and J. F. Carpentier, *Coord. Chem. Rev.*, 2008, **252**, 2137-2154.
- 18 D. A. X. Fraser, Z. R. Turner, J.-C. Buffet and D. O'Hare, *Organometallics*, 2016, **35**, 2664-2674.
- 19 P. C. Mohring and N. J. Coville, *Coord. Chem. Rev.*, 2006, **250**, 18-35.
- 20 N. E. Grimmer, N. J. Coville and C. B. de Koning, *J. Organomet. Chem.*, 2002, **642**, 195-202.
- 21 C. H. Rochester, *J. Chem. Technol. Biotechnol.*, 1996, **65**, 105-105.

- 22 T. E. Ready, J. C. W. Chien and M. D. Rausch, *J. Organomet. Chem.*, 1996, **519**, 21-28.
- 23 T. E. Ready, R. O. Day, J. C. W. Chien and M. D. Rausch, *Macromolecules*, 1993, **26**, 5822-5823.
- 24 T. K. Miyamoto, M. Tsutsui and L. B. Chen, *Chem. Lett.*, 1981, 729-730.
- 25 F. M. Alías, S. Barlow, J. S. Tudor, D. O'Hare, R. T. Perry, J. M. Nelson and I. Manners, *J. Organomet. Chem.*, 1997, **528**, 47-58.
- 26 (a) D. O'Hare and J.-C. Buffet, WO2016075485A1, 2016. (b) D. O'Hare, J.-C. Buffet, J. E. Matley and C. M. R. Wright, WO2017194943A1, 2017.
- 27 J. Lamb, D. O'Hare, J.-C. Buffet, T. Khamnaen, M. Charernsuk, T. Parawan and S. Charoenchaidet, WO2017194943A1, 2017.
- 28 W. J. Gauthier, J. F. Corrigan, N. J. Taylor and S. Collins, *Macromolecules*, 1995, **28**, 3771-3778.
- 29 W. Kaminsky, *Macromol. Chem. and Phys.*, 1996, **197**, 3907-3945.
- 30 T. A. Q. Arnold, Z. R. Turner, J.-C. Buffet and D. O'Hare, *J. Organomet. Chem.*, 2016, **822**, 85-90.
- 31 A. F. R. Kilpatrick, J.-C. Buffet, P. Nørby, N. H. Rees, N. P. Funnell, S. Sripothongnak and D. O'Hare, *Chem. Mater.*, 2016, **28**, 7444-7450.
- 32 J.-C. Buffet, N. Wanna, T. A. Q. Arnold, E. K. Gibson, P. P. Wells, Q. Wang, J. Tantirungrotechai and D. O'Hare, *Chem. Mater.*, 2015, **27**, 1495-1501.
- 33 J.-C. Buffet, Z. R. Turner, R. T. Cooper and D. O'Hare, *Polym. Chem.*, 2015, **6**, 2493-2503.
- 34 M. M. Mortazavi, S. Ahmadjo, J. H. Z. Dos Santos, H. Arabi, M. Nekoomanesh, G. H. Zohuri, R. Brambilla and G. B. Galland, *J. Appl. Polym. Sci.*, 2013, **130**, 4568-4575.
- 35 D. Bianchini, J. H. Z. dos Santos, T. Uozumi and T. Sano, *J. Mol. Catal. A-Chem.*, 2002, **185**, 223-235.
- 36 P. Angpanitcharoen, G. Hay, J.-C. Buffet, Z. R. Turner, T. A. Q. Arnold and D. O'Hare, *Polyhedron*, 2016, **116**, 216-222.
- 37 I. M. Lee, W. J. Gauthier, J. M. Ball, B. Iyengar and S. Collins, *Organometallics*, 1992, **11**, 2115-2122.
- 38 G. Sivalingam, V. Natarajan, K. R. Sarma and U. Parasuveera, *Ind. Eng. Chem. Res.*, 2008, **47**, 8940-8946.
- 39 M. A. Parvez, M. Rahaman, M. A. Suleiman, J. B. P. Soares and I. A. Hussein, *Int. J. Polym. Sci.*, 2014, 1-10.
- 40 (a) M. Eskelinen and J. V. Seppala, *Eur. Polym. J.*, 1996, **32**, 331-335. (b) V. R. Gowariker, N. V. Viswanathan and J. Sreedhar, Wiley, 1986, ch. 4, pp. 105-135.
- 41 (a) J.-C. Buffet, Z. R. Turner and D. O'Hare, *Chem. Commun.*, 2018, **54**, 10970-10973. (b) T. J. Williams, J.-C. Buffet, Z. R. Turner and D. O'Hare, *Catal. Sci. Technol.*, 2018, **8**, 5454-5461.
- 42 J. E. O'Hara and K. B. Wagener, *Makromolekulare Chemie-Rapid Communications*, 1993, **14**, 657-662.
- 43 G. Rojas, B. Inci, Y. Wei and K. B. Wagener, *J. Am. Chem. Soc.*, 2009, **131**, 17376-17386.
- 44 F. M. Mirabella and A. Bafna, *J. Polym. Sci., Part B: Polym. Phys.*, 2002, **40**, 1637-1643.
- 45 J.-C. Buffet, C. F. H. Byles, R. Felton, C. P. Chen and D. O'Hare, *Chem. Commun.*, 2016, **52**, 4076-4079.
- 46 I. Silanes, J. M. Mercero and J. M. Ugalde, *Organometallics*, 2006, **25**, 4483-4490.